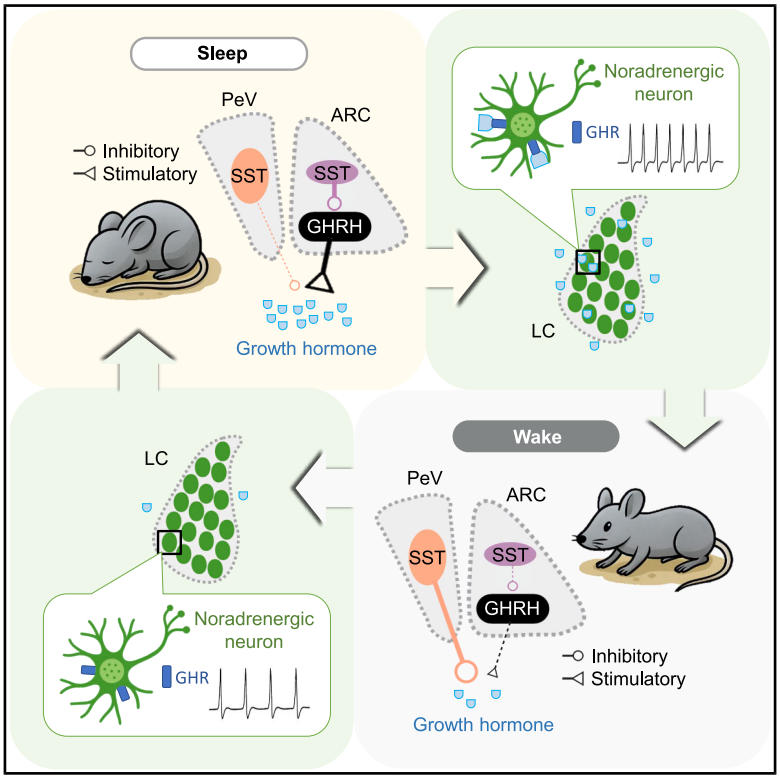
Cell

Article

Neuroendocrine circuit for sleep-dependent growth hormone release

Graphical abstract



Authors

Xinlu Ding, Fuu-Jiun Hwang, Daniel Silverman, ..., Zhiyu Melissa Tian, Jun Ding, Yang Dan

Correspondence

ydan@berkeley.edu

In brief

The increase in growth hormone release during sleep is driven by sleep-wake-dependent activity of stimulatory GHRH neurons and inhibitory SST neurons in the hypothalamus. The released growth hormone enhances the excitability of locus coeruleus noradrenergic neurons and promotes wakefulness, revealing an additional negative feedback pathway.

Highlights

- Sleep-dependent GH release is regulated by distinct GHRH and SST hypothalamic neurons
- SST neurons in ARC suppress GH release by inhibiting GHRH neurons that are stimulatory
- SST neurons in PeV suppress GH release through their projections to the median eminence
- Feedback pathway with GH enhancing LC neuron excitability and promoting wakefulness

Ding et al., 2025, Cell *188*, 1–12
September 4, 2025 © 2025 The Authors. Published by Elsevier Inc.
https://doi.org/10.1016/j.cell.2025.05.039

CellPress

Please cite this article in press as: Ding et al., Neuroendocrine circuit for sleep-dependent growth hormone release, Cell (2025), https://doi.org/10.1016/j.cell.2025.05.039

Cell

CellPress
OPEN ACCESS

Article

Neuroendocrine circuit for sleep-dependent growth hormone release

Xinlu Ding,[1] Fuu-Jiun Hwang,[2] Daniel Silverman,[1] Peng Zhong,[1,4] Bing Li,[1] Chenyan Ma,[1] Lihui Lu,[1] Grace Jiang,[1] Zhe Zhang,[1,5] Xiaolin Huang,[1] Xun Tu,[1] Zhiyu Melissa Tian,[1] Jun Ding,[2,3] and Yang Dan[1,6,*]

[1]Division of Neurobiology, Department of Molecular and Cell Biology, Helen Wills Neuroscience Institute, Howard Hughes Medical Institute, University of California, Berkeley, CA 94720, USA
[2]Department of Neurosurgery, Stanford University, Stanford, CA 94305, USA
[3]Department of Neurology and Neurological Science, Stanford University, Stanford, CA 94305, USA
[4]Present address: Department of Neurological Sciences, University of Nebraska Medical Center, Omaha, NE 68106, USA
[5]Present address: Institute of Neuroscience, State Key Laboratory of Neuroscience, Key Laboratory of Primate Neurobiology, Center for Excellence in Brain Science and Intelligence Technology, Chinese Academy of Sciences, Shanghai 200031, China
[6]Lead contact
*Correspondence: ydan@berkeley.edu
https://doi.org/10.1016/j.cell.2025.05.039

SUMMARY

Sleep is known to promote tissue growth and regulate metabolism, partly by enhancing growth hormone (GH) release, but the underlying circuit mechanism is unknown. We demonstrate how GH release, which is enhanced during both rapid eye movement (REM) and non-REM (NREM) sleep, is regulated by sleep-wake-dependent activity of distinct hypothalamic neurons expressing GH-releasing hormone (GHRH) and somatostatin (SST). SST neurons in the arcuate nucleus suppress GH release by inhibiting nearby GHRH neurons that stimulate GH release, whereas periventricular SST neurons inhibit GH release by projecting to the median eminence. GH release is associated with strong surges of both GHRH and SST activity during REM sleep but moderately increased GHRH and decreased SST activity during NREM sleep. Furthermore, we identified a negative feedback pathway in which GH enhances the excitability of locus coeruleus neurons and increases wakefulness. These results elucidate a circuit mechanism underlying bidirectional interactions between sleep and hormone regulation.

INTRODUCTION

Sleep is a vital process for rejuvenating the body and brain, and sleep deficits are linked to numerous health problems. In addition to cognitive and emotional impairments, insufficient sleep can increase the risks of diabetes, obesity, and cardiovascular diseases.[1–3] An important mechanism by which sleep can influence a wide range of tissues and organs is neuroendocrine regulation. Sleep deprivation has been shown to disrupt the balance of multiple hormones.[4–6]

Growth hormone (GH) is known to promote protein synthesis, stimulate lipolysis, and regulate glucose homeostasis,[7,8] and it plays essential roles in muscle and bone growth during both development and adulthood.[9–12] GH deficiency can result in reduced lean body mass, increased visceral fat, insulin resistance, and increased cardiovascular risk,[13] resembling many detrimental effects of sleep deprivation.[1–3] GH release has been shown to be closely associated with sleep.[14–17] However, the mechanism underlying the interaction between sleep and GH signaling remains unclear.

To address this knowledge gap, we investigated how sleep influences the activity of the GH-controlling neuroendocrine circuit and how GH signaling, in turn, affects sleep. The production and release of GH by somatotroph cells in the anterior pituitary are known to be stimulated by GH-releasing hormone (GHRH)[18,19] and inhibited by somatostatin (SST)[20] peptides, which are released by distinct neuronal populations in the hypothalamus. Using optogenetic and chemogenetic manipulations, we characterized the causal relationships between the activity of hypothalamic GHRH and SST neurons and GH release. Calcium photometry and optrode recording showed that the activity of both GHRH and SST neurons in the hypothalamus is modulated by sleep-wake states, revealing distinct mechanisms for enhanced GH release during rapid eye movement (REM) and non-REM (NREM) sleep. Furthermore, we identified a previously unrecognized negative feedback pathway in which GH enhances the excitability of noradrenergic neurons in the locus coeruleus (LC) and promotes wakefulness.

RESULTS

Sleep enhances GHRH-induced GH release

The GHRH peptide that stimulates GH release[18,19] originates primarily from a population of neurons in the arcuate nucleus (ARC)

This is an open access article under the CC BY license (http://creativecommons.org/licenses/by/4.0/).

Please cite this article in press as: Ding et al., Neuroendocrine circuit for sleep-dependent growth hormone release, Cell (2025), https://doi.org/10.1016/j.cell.2025.05.039

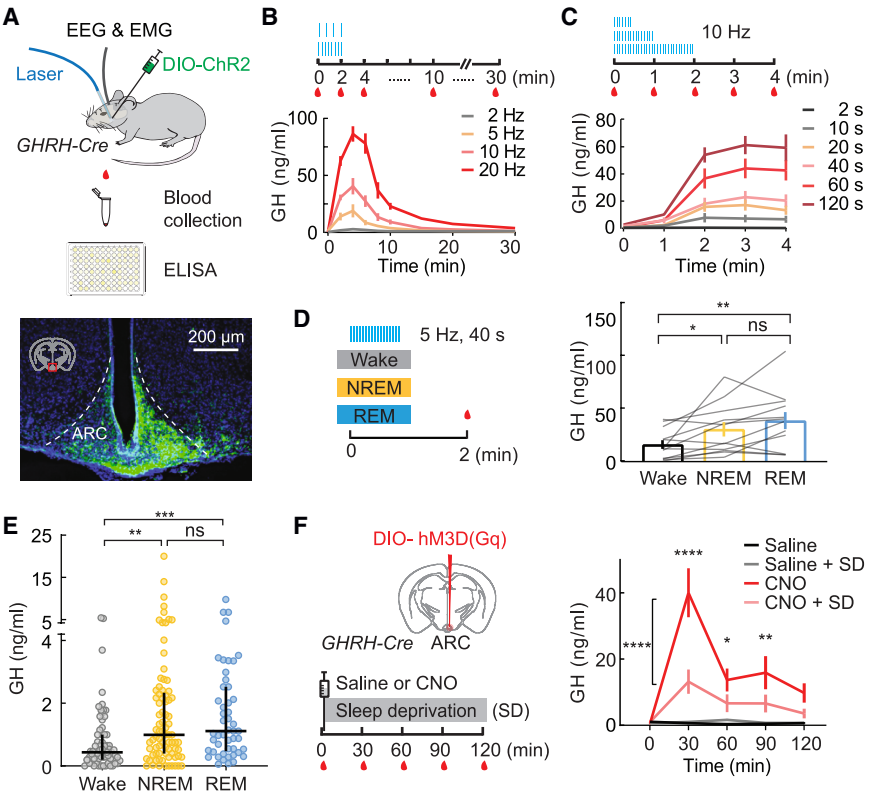


Figure 1. Sleep enhances GHRH-induced GH release

(A) Top, schematic of optogenetic stimulation, blood collection, and GH measurement by ELISA. Bottom, fluorescence image of ARC (red box in coronal diagram) showing ChR2-eYFP expression in a *GHRH-Cre* mouse.

(B) Mean GH levels in blood before and at 2, 4, 6, 8, 10, 15, 20, and 30 min after optogenetic stimulation for 2 min at different frequencies. $n = 5$ mice (4 male, 1 female).

(C) Mean GH levels in blood before and 1, 2, 3, and 4 min after optogenetic stimulation at 10 Hz for different durations. $n = 6$ mice (4 male, 2 female).

(D) Left, schematic. Right, GH levels were measured 2 min after 40 s of optogenetic stimulation applied during wake, NREM, or REM sleep ($n = 12$ mice, 8 male and 4 female). p (wake vs. NREM) = 0.046, p (wake vs. REM) = 0.0014, p (NREM vs. REM) = 0.45 (one-way repeated measures ANOVA with Bonferroni correction). Bar and error bars, mean ± SEM.

(E) Blood GH levels during or shortly after each sleep-wake state. wake, $n = 67$ samples; NREM, $n = 81$; REM, $n = 49$; from 13 mice (5 male, 8 female). p (wake vs. NREM) = 0.001, p (wake vs. REM) = 0.0005, p (NREM vs. REM) > 0.99 (Kruskal-Wallis test followed by Dunn's test). Horizontal bar, median; vertical bar, first (top) and third (bottom) quartiles.

(F) Left, schematic of ARC expressing hM3D(Gq)-mCherry in GHRH neurons. Mean GH levels were measured before and after saline or CNO injection, with or without sleep deprivation. $n = 6$ mice (4 male, 2 female). 30 min: p (saline vs. CNO+SD) = 0.011, p (saline vs. CNO) < 0.0001, p (CNO vs. CNO+SD) < 0.0001; 60 min: p (saline vs. CNO) = 0.023; 90 min: p (saline vs. CNO) = 0.006 (two-way repeated measures ANOVA with Bonferroni correction).

Error bar, ± SEM. *$p < 0.05$; **$p < 0.01$; ***$p < 0.001$; ****$p < 0.0001$; ns, not significant.

See also Figure S1.

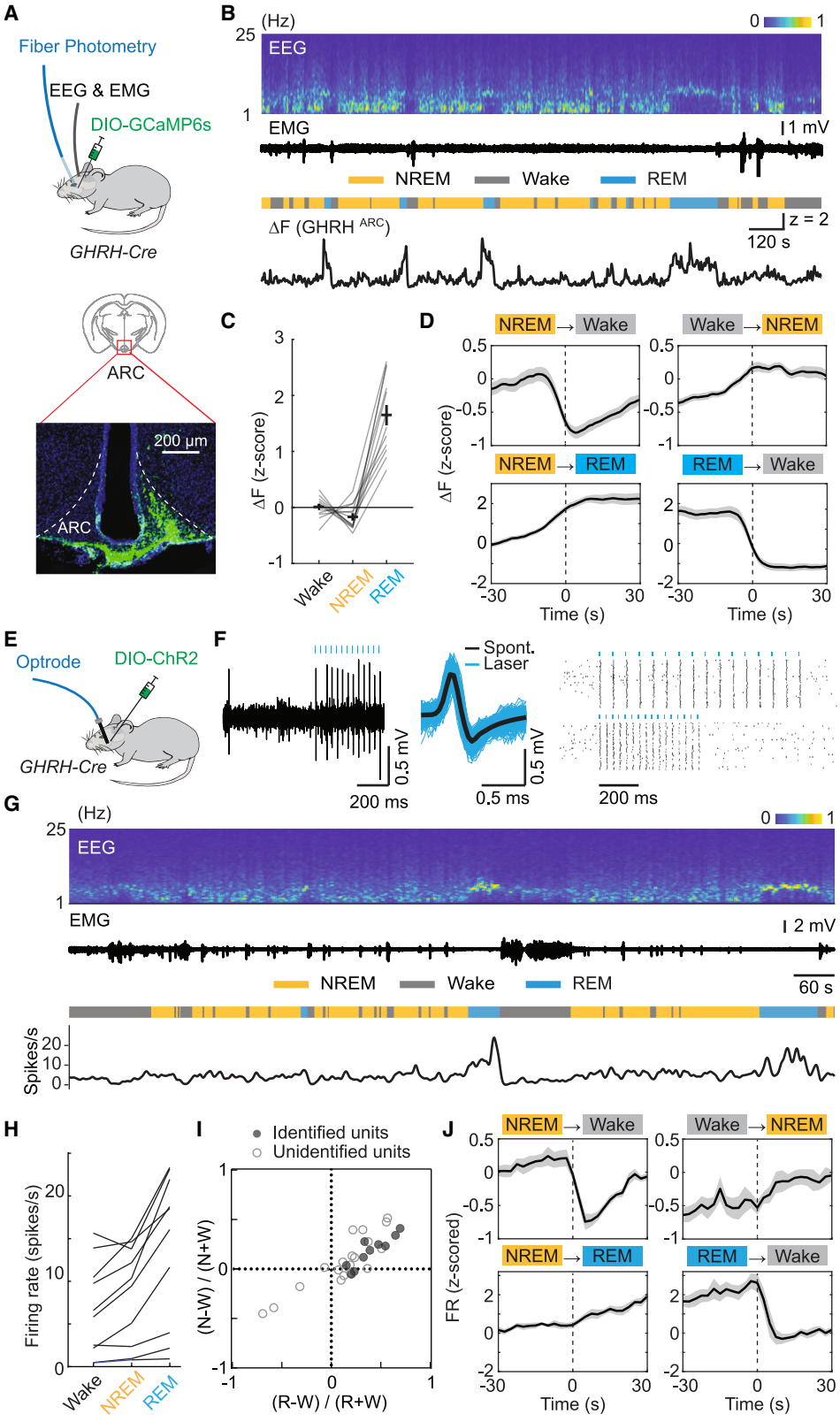
of the hypothalamus.[21] To quantify the relationship between GHRH neuron activity and GH release, we injected Cre-inducible adeno-associated virus (AAV) expressing channelrhodopsin-2 (ChR2) fused with enhanced yellow fluorescent protein (eYFP) (AAV-double-floxed inverse orientation [DIO]-ChR2-eYFP) into the ARC of *GHRH-Cre* mice.[22] Optogenetic stimulation was applied in freely moving mice for 2 min over a range of frequencies (2, 5, 10, and 20 Hz), and blood samples were collected from the tail before and after the stimulation; GH levels in the blood were measured using enzyme-linked immunosorbent assay (ELISA)[23] (Figures 1A and 1B). We found a rapid increase in the GH level after stimulation, which reached the peak ~2 min after the stimulation and decayed over the next several minutes. The level of GH increased monotonically with the frequency of stimulation between 2 and 20 Hz (Figure 1B). Similarly, when the frequency was fixed at 10 Hz, the amount of GH release increased with the duration of stimulation (Figure 1C). Thus, activation of ARC GHRH neurons rapidly triggered GH release in a frequency- and duration-dependent manner.

We next tested whether the GH release evoked by GHRH neuron activation is modulated by sleep-wake brain states, classified based on electroencephalogram (EEG) and electromyogram (EMG) recordings. We applied optogenetic stimulation at 5 Hz, which caused no significant change in brain states (Figures S1A–S1C), and collected blood samples 2 min after each stimulation trial (40 s/trial, Figure 1D). Interestingly, evoked GH release was significantly higher for laser stimulation applied during REM and NREM sleep than during wakefulness (REM, $p = 0.0014$; NREM, $p = 0.046$, one-way repeated measures ANOVA with Bonferroni correction), indicating that the efficacy of GHRH neuron activity in stimulating GH release is modulated by brain states. We also measured the endogenous GH release without GHRH neuron stimulation and found that the GH level was significantly higher during or shortly after (<1 min) REM or NREM episodes compared with wakefulness (Figure 1E; REM, $p = 0.0005$; NREM, $p = 0.001$; Kruskal-Wallis test followed by Dunn's test), with no significant difference between male and female mice (Figure S1D). Thus, both endogenous and GHRH-activation-induced GH release are enhanced by NREM and REM sleep, although on average the endogenous GH levels are much lower than the induced GH release. It is also worth noting that, although the overall GH levels are similar during NREM and REM sleep, mice generally spend much more time in NREM than REM sleep. Thus, the bulk of GH release is likely to occur during NREM sleep.[15,16]

We then tested the effect of sleep on GH release evoked by chemogenetic activation of GHRH neurons. In *GHRH-Cre* mice injected with AAV-DIO-hM3D(Gq)-mCherry in the ARC, clozapine N-oxide (CNO) but not saline caused a strong increase in the GH level, which lasted for 1–2 h (Figures 1F and S1E). However, in mice completely deprived of sleep following

Please cite this article in press as: Ding et al., Neuroendocrine circuit for sleep-dependent growth hormone release, Cell (2025), https://doi.org/10.1016/j.cell.2025.05.039

CellPress
OPEN ACCESS



(legend on next page)

Please cite this article in press as: Ding et al., Neuroendocrine circuit for sleep-dependent growth hormone release, Cell (2025), https://doi.org/10.1016/j.cell.2025.05.039

CNO injection, the GH level was significantly lower than in the mice allowed to sleep freely ($p < 0.0001$, two-way repeated measures ANOVA with Bonferroni correction). Consistent with the previous finding that the GHRH peptide can promote sleep,[24–26] we found that chemogenetic activation of GHRH neurons significantly increased NREM sleep (Figure S1F). Given the impact of sleep on enhancing optogenetically and chemogenetically evoked GH release (Figures 1D and 1F), the sleep-promoting effect of GHRH peptide may provide an additional mechanism for enhancing GH release induced by GHRH neuron activity.

GHRH neuron activity during sleep and wakefulness

Having characterized the efficacy of GHRH neuron activity in inducing GH release using opto- and chemogenetic stimulation, we next measured the endogenous activity of GHRH neurons across sleep-wake states. Cre-inducible AAV expressing the calcium indicator GCaMP6s (AAV-DIO-GCaMP6s) was injected into the ARC of *GHRH-Cre* mice, and calcium activity was measured using fiber photometry (Figure 2A). ARC GHRH neurons were most active during REM sleep, with the strongest increase in calcium activity at the NREM→REM transition and decrease at the REM→wake transition (Figures 2B–2D). We also observed a consistent increase at the wake→NREM transition and a decrease at the NREM→wake transition, although these NREM-related changes were considerably smaller than those associated with REM sleep.

In addition to calcium photometry, we also measured the firing rates of GHRH neurons using optrode recordings in the ARC of *GHRH-Cre* mice injected with AAV-DIO-ChR2-eYFP (Figure 2E). High-frequency laser pulses (15 or 30 Hz; 5 ms per pulse; 16 pulses per train) were applied intermittently, and single units exhibiting reliable laser-evoked spiking at short latencies and low jitter were identified as GHRH neurons (Figure 2F). All of the identified GHRH neurons ($n = 10$) exhibited the highest firing rates during REM sleep (Figures 2G–2I), and at the population level the firing rates were significantly higher during REM sleep than during both NREM sleep and wakefulness (REM vs. NREM, $p = 0.0007$; REM vs. wake, $p < 0.0001$, one-way repeated measures ANOVA with Bonferroni correction). The firing rate changes at brain state transitions were also similar to those observed with calcium fiber photometry (Figure 2J). Optogenetic inhibition of ARC GHRH neurons during REM and NREM sleep suppressed endogenous GH release, suggesting that GHRH neuron activity is necessary for sleep-dependent GH secretion (Figure S2).

Regulation of GH release by two SST neuron populations

Given the much higher activity of GHRH neurons during REM than NREM sleep (Figures 2C, 2D, and 2H–2J), we wondered why the mean GH levels were similar between the two sleep states (Figure 1E). In addition to GHRH, GH release is also regulated by SST, which acts on both pituitary somatotrophs[20] and GHRH neurons.[27]

First, to identify the SST neurons innervating ARC GHRH neurons, we performed rabies virus (RV)-mediated transsynaptic retrograde tracing by injecting AAVs expressing an avian retroviral receptor (TVA) fused with mCherry (TC, AAV-chicken beta-actin promoter [CAG]-flipping excision [FLEx]-TC66T, or AAV-CAG-FLEx-TCB) and a rabies glycoprotein (RG) (AAV-CAG-FLEx-RG) into the ARC of *GHRH-Cre* mice; a modified RV expressing enhanced green fluorescent protein (EGFP) (glycoprotein-deleted rabies virus [RVdG]-EGFP+EnvA) was injected 3 weeks later. We found many RV-labeled SST-expressing presynaptic neurons in the ARC but far fewer in the periventricular nucleus (PeV) of the hypothalamus (Figures 3A, S3A, and S3B). Next, to identify the endocrine cells that release SST into the pituitary, we injected Fluorogold (FG) subcutaneously, which efficiently tags neuroendocrine cells that project outside the blood-brain barrier.[28,29] We found much greater labeling of SST neurons in the PeV than the ARC (Figure 3B), consistent with previous reports identifying the PeV as a major source of SST for the pituitary.[30,31] Anterograde tracing of axon projections using mCherry further confirmed that SST neurons in the PeV but not the ARC send extensive projections to the median eminence (ME, Figures 3C and S3C). These results reveal two populations of SST neurons that may regulate GH release through distinct projections.

Virtually all ARC SST neurons expressed the vesicular gamma-aminobutyric acid (GABA) transporter *vGat* (encoded by *Slc32a1*, Figure 4A), suggesting that in addition to SST, they also use GABA as a neurotransmitter. To measure the functional interaction between ARC SST and GHRH neurons, we injected both AAV-DIO-GCaMP6s and AAV-fDIO-ChrimsonR into the

Figure 2. Dependence of GHRH neuron activity on sleep-wake states

(A) Top, schematic of calcium fiber photometry recording of GHRH neuron calcium activity. Bottom, fluorescence image of ARC (red box in coronal diagram) expressing GCaMP6s.

(B) An example session with EEG spectrogram, EMG trace, brain states (color-coded), and calcium activity of GHRH neurons.

(C) Mean calcium activity of GHRH neurons in each brain state. Each line represents one mouse. $n = 12$ mice. p (wake vs. NREM) = 0.50; p (REM vs. NREM) < 0.0001; p (REM vs. wake) < 0.0001 (one-way repeated measures ANOVA with Bonferroni correction).

(D) Mean calcium activity of GHRH neurons at brain state transitions ($n = 12$ mice). Time 0 indicates the transition point.

(E) Schematic of optrode recording from GHRH neurons in freely moving mice.

(F) Example recording of spontaneous and laser-evoked spikes from an identified GHRH neuron. Left: raw trace. Blue ticks, laser pulses. Middle: comparison of laser-evoked (blue) and averaged spontaneous (black) spike waveforms. Right: spike raster showing multiple laser stimulation trials at 15 and 30 Hz.

(G) An example session with EEG spectrogram, EMG trace, brain states (color-coded), and firing rate of an example GHRH neuron.

(H) Firing rates of 10 identified GHRH neurons during different brain states. Each line shows the firing rates of one neuron. p (wake vs. NREM) = 0.55; p (REM vs. NREM) = 0.0007; p (REM vs. wake) < 0.0001 (one-way repeated measures ANOVA with Bonferroni correction).

(I) REM-wake vs. NREM-wake activity differences (Z scored firing rates) of all identified GHRH (solid circle, $n = 10$ neurons from 4 mice) and unidentified (open circle, $n = 19$ neurons from 4 mice) neurons in the ARC.

(J) Mean firing rate (Z scored) of all identified GHRH neurons at brain state transitions ($n = 10$ neurons from 4 mice). Time 0 indicates the transition point.

Error bar, ± SEM. Shading, ± SEM.

See also Figure S2.

Please cite this article in press as: Ding et al., Neuroendocrine circuit for sleep-dependent growth hormone release, Cell (2025), https://doi.org/10.1016/j.cell.2025.05.039

CellPress
OPEN ACCESS

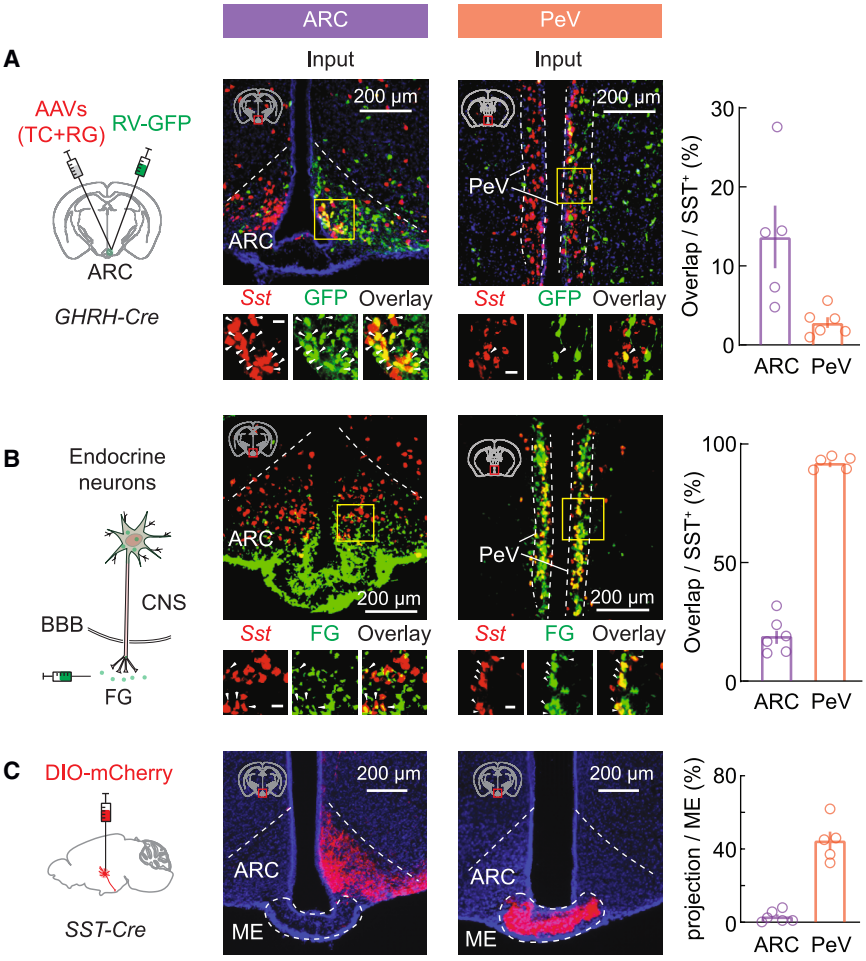


Figure 3. ARC and PeV SST neurons project to distinct downstream targets

(A) Left, schematic showing rabies-mediated transsynaptic tracing from ARC GHRH neurons. Middle, overlap between *Sst* mRNA and rabies-labeled presynaptic neurons in the ARC (left) and PeV (right). Region in yellow box is shown below. Arrowheads indicate co-labeled neurons. Scale bar, 25 μm. Right, bar graph showing the percentages of SST neurons labeled with rabies GFP in the ARC (n = 5 mice) and PeV (n = 6 mice). Each circle represents one mouse.

(B) Left, schematic showing fluorogold (FG) labeling of neuroendocrine neurons projecting outside the blood-brain barrier (BBB). Middle, overlap between *Sst* mRNA and FG in the ARC (left) and PeV (right). Region in yellow box is shown below. Arrowheads indicate co-labeled neurons. Scale bar, 25 μm. Right, bar graph showing the percentages of SST neurons that are co-labeled with FG in the ARC (n = 6 mice) and PeV (n = 5 mice). Each circle represents one mouse.

(C) Left, schematic of anterograde tracing. Middle, example fluorescence images of *SST-Cre* mice injected with AAV-DIO-mCherry in the ARC (left, showing little projection to the ME) or PeV (right, showing strong projection to the ME). Right, bar graph showing the percentage of ME area receiving ARC (n = 6 mice) or PeV (n = 5 mice) SST neuron projections. Each circle represents one mouse.

Bar and error bar, mean ± SEM.

See also Figure S3.

ARC of *SST-Flp* crossed with *GHRH-Cre* (*SST-Flp;GHRH-Cre*) mice (Figure 4B). Optogenetic stimulation (10 mW/mm^2, 20 Hz) and photometry recording through the same optic fiber showed that SST neuron activation caused an immediate decrease in GHRH neuron calcium activity without changing the brain state (Figures 4C–4E and S4A–S4C). In control mice expressing GCaMP6s in GHRH neurons but not ChrimsonR in SST neurons, laser stimulation had no effect (Figures S4D–S4F), and the laser-induced decrease in GHRH neuron activity was significantly different between ChrimsonR and control groups (Figure 4E, p = 0.0022, t test). These experiments confirmed a local inhibition of GHRH neurons by SST neurons within the ARC.

We then tested the role of these SST neurons in regulating GH release by injecting AAV-hSyn-DIO-hM4D(Gi)-mCherry into the ARC of *SST-Cre* mice. We found a marked increase in the blood GH level 15 min after CNO but not saline injection (Figures 4F and S4G). Chemogenetic inhibition of PeV SST neurons also caused a strong increase in GH level (Figures 4G and S4H). Thus, both populations of SST neurons strongly inhibit GH release, albeit through different circuit mechanisms (Figure 4H): either by inhibiting the GHRH neurons that stimulate GH release or by releasing SST into the pituitary to counteract the effect of GHRH on somatotrophs.

SST neuron activity during sleep and wakefulness

Next, we measured the endogenous activity of both SST populations across sleep-wake cycles. To compare the activity of PeV SST and ARC GHRH neurons directly, we recorded from the two populations simultaneously using dual calcium fiber photometry. In *SST-Flp;GHRH-Cre* mice, we injected AAV-fDIO-GCaMP6s into the PeV of one hemisphere and AAV-DIO-GCaMP6s into the ARC of the other hemisphere (Figure 5A). Similar to ARC GHRH neurons, PeV SST neurons showed a rapid increase and decrease in activity at the onset and termination of REM sleep, respectively (Figures 5B–5D). Unlike GHRH neurons, however, SST neurons showed a small increase in activity at the NREM→wake transition and a decrease at the wake→NREM transition. Thus, although GH release is increased during both REM and NREM sleep, they appear to be regulated differently. During REM sleep, GH release is triggered by a powerful surge of ARC GHRH activity counterbalanced by a strong increase in PeV SST activity. During NREM sleep, however, it is caused by moderate activity changes of both populations but in opposite directions: an increase in GHRH activity and a decrease in SST activity (Figure 5D).

We then measured ARC SST neuron activity by injecting AAV-DIO-GCaMP6s into *SST-Cre* mice (Figure 5E). These neurons exhibited activity profiles similar to those of GHRH neurons across brain states (Figures 5F–5H). The strong similarity

Please cite this article in press as: Ding et al., Neuroendocrine circuit for sleep-dependent growth hormone release, Cell (2025), https://doi.org/10.1016/j.cell.2025.05.039

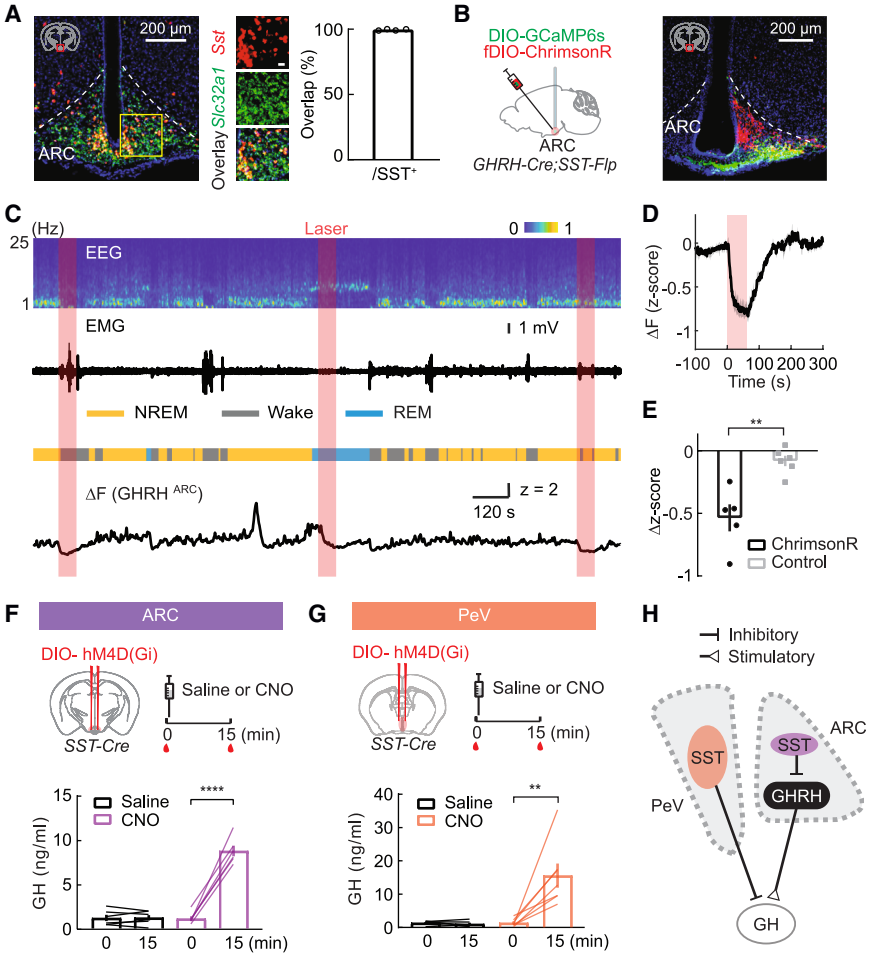


Figure 4. Inhibition of GH release by ARC and PeV SST neurons

(A) Overlap between *Sst* and *vGat* mRNA in the ARC. Yellow-boxed region is shown on the right. Scale bar, 25 μm. The bar graph shows the percentage of SST neurons expressing *vGat*. Each circle represents one mouse (n = 4 mice).

(B) Left, schematic of calcium fiber photometry and optogenetic manipulation through the same fiber. Right, fluorescence image of ARC (red box in coronal diagram) expressing fDIO-ChrimsonR-tdTomato and DIO-GCaMP6s in a *GHRH-Cre; SST-Flp* mouse.

(C) An example session with EEG spectrogram, EMG trace, brain states (color-coded), and calcium activity of GHRH neurons. Red stripe, laser stimulation period (20 Hz, 60 s).

(D) Mean calcium activity of GHRH neurons before, during, and after optogenetic activation of SST neurons (n = 5 mice). Red stripe, laser stimulation period (20 Hz, 60 s).

(E) Changes in mean response amplitude induced by laser stimulation in mice with or without ChrimsonR expression. Each circle or square represents one mouse (ChrimsonR$^+$, n = 5 mice; ChrimsonR$^-$, n = 6 mice). p = 0.0022 (t test).

(F) Top, schematic of chemogenetic inactivation. Bottom, GH levels were measured before and 15 min after saline (n = 6 mice) or CNO injection (n = 7 mice) in mice expressing hM4D(Gi)-mCherry in ARC SST neurons. $p < 0.0001$ (paired t test).

(G) Similar to (F), but for mice expressing hM4D (Gi)-mCherry in PeV SST neurons (n = 6 mice). p = 0.0089 (paired t test).

(H) Diagram summarizing the circuit mechanism regulating GH release.

Bar and error bar, mean ± SEM. Shading, ± SEM. $^{**}p < 0.01$; $^{****}p < 0.0001$.

See also Figure S4.

between SST and GHRH neuron activity suggests that the ARC SST neurons provide balanced inhibition of GHRH neurons.

To further examine the role of SST neuron activity in regulating brain-state-dependent GH release, we injected AAV-DIO-ChR2-eYFP into the PeV or ARC of *SST-Cre* mice. Optogenetic activation of either PeV or ARC SST neurons during NREM sleep, when their natural activity is low (Figures 5C and 5G), significantly reduced GH release (Figures S5A and S5B), indicating that the reduction of their activity is important for increased GH release during NREM sleep.

GH regulation of noradrenergic neuron activity and sleep

Having examined the circuit mechanism for sleep-dependent GH release, we next explored the effects of GH signaling on sleep-wake regulation. *In situ* hybridization with RNAscope showed strong expression of GH receptors (GHRs) in several areas of the hypothalamus (Figure S6A), which are known to regulate glucose metabolism, energy homeostasis, as well as GH synthesis and release.[32–35] Interestingly, GHR expression was also observed in neurons with crucial roles in wakefulness and arousal, including dopaminergic neurons in the midbrain and noradrenergic neurons in the LC[36,37] (Figures 6A and S6B). This raises the possibility that, in addition to being regulated by sleep, GH release can in turn influence sleep-wake states. Given the well-established effect of LC neurons in promoting wakefulness and suppressing both REM and NREM sleep,[38–40] we focused on the effect of GH signaling on LC neurons.

First, we tested the effect of intravenous injection of GH on LC neurons. Compared with saline control, GH injection induced a strong increase in c-FOS expression in LC noradrenergic neurons (Figure 6B), suggesting an increase in their activity *in vivo*. To test whether this is mediated by GHRs expressed in LC noradrenergic neurons, we used CRISPR/SaCas9-mediated genome editing to knock down GHR expression. In dopamine beta-hydroxylase (*DBH*)-*Cre* mice, injection of AAV with Cre-dependent expression of SaCas9 and a single guide RNA (sgRNA) targeting the *Ghr* gene (AAV-FLEX-SaCas9-sgGHR) into the LC caused a marked reduction of *Ghr* expression compared with control mice injected with AAV-FLEX-SaCas9-sgROSA26 (Figure S6C). GH-induced c-FOS expression was also significantly reduced (Figure 6D), indicating that the increased activity depends on GHRs expressed in LC neurons.

Please cite this article in press as: Ding et al., Neuroendocrine circuit for sleep-dependent growth hormone release, Cell (2025), https://doi.org/10.1016/j.cell.2025.05.039

CellPress
OPEN ACCESS

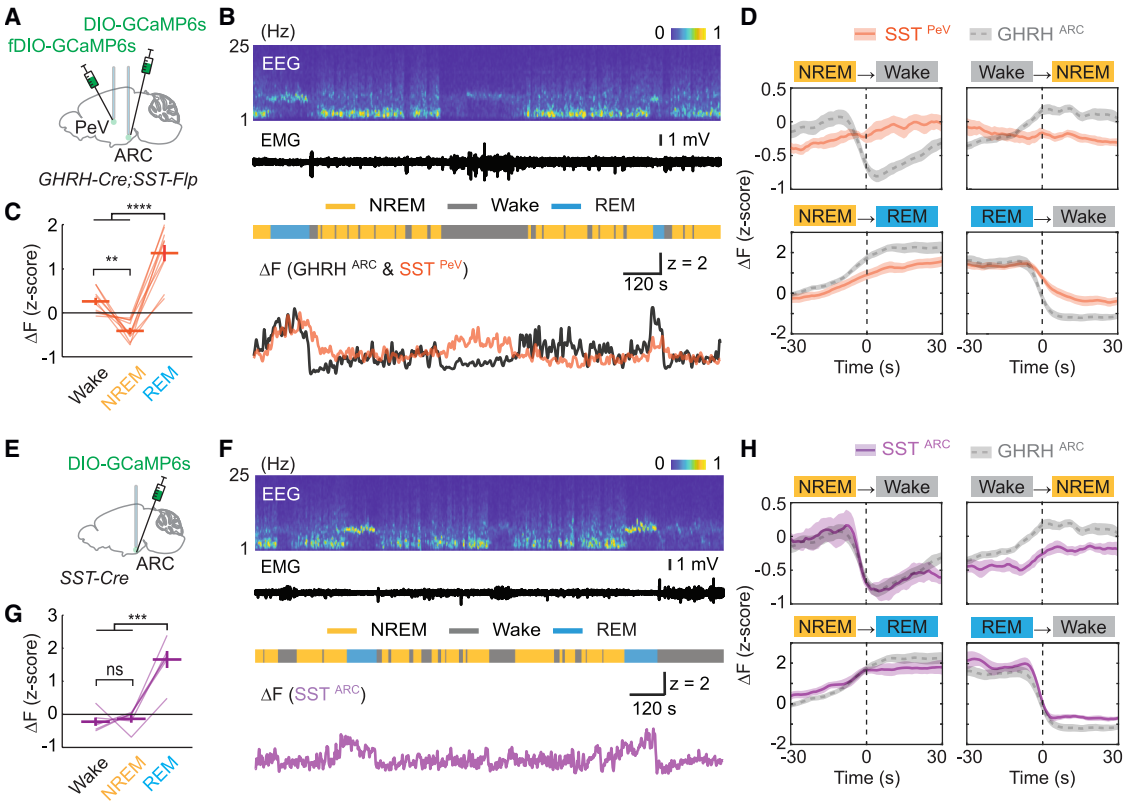


Figure 5. Dependence of SST neuron activity on sleep-wake states

(A) Schematic of dual calcium fiber photometry.

(B) An example session with EEG spectrogram, EMG trace, brain states (color-coded), and calcium activity of ARC GHRH neurons (black) and PeV SST neurons (orange).

(C) Mean calcium activity of PeV SST neurons in each brain state. Each line represents one mouse (n = 10 mice). p (wake vs. NREM) = 0.0087; p (REM vs. NREM) < 0.0001; p (REM vs. wake) < 0.0001 (one-way repeated measures ANOVA with Bonferroni correction).

(D) Mean calcium activity of PeV SST neurons (red line, n = 10 mice) at brain state transitions superimposed on GHRH neuron activity (gray dashed line, n = 12 mice, same as Figure 5H). Dual calcium fiber photometry recording from both SST and GHRH neurons was performed in 5 mice. Time 0 indicates the transition point.

(E) Schematic of calcium fiber photometry recording of ARC SST neurons' calcium activity.

(F) An example session with EEG spectrogram, EMG trace, brain states (color-coded), and calcium activity of ARC SST neurons.

(G) Mean calcium activity of ARC SST neurons in each brain state. Each line represents one mouse (n = 6 mice). p (wake vs. NREM) > 0.99; p (REM vs. NREM) = 0.0002; p (REM vs. wake) = 0.0001 (one-way repeated measures ANOVA with Bonferroni correction).

(H) Similar to (D), but for activity of ARC SST neurons (magenta line, n = 6 mice).

Error bar, ± SEM. Shading, ± SEM. **p < 0.01; ***p < 0.001; ****p < 0.0001; ns, not significant.

See also Figure S5.

We next made whole-cell patch-clamp recordings from noradrenergic neurons labeled with EGFP in acute LC slices from *DBH-Cre* mice. For each LC neuron, we injected a series of current steps (0–200 pA, with an increment of 50 pA) to test if GH affects the intrinsic excitability of noradrenergic neurons (Figure 6E). In control mice (injected with AAV-FLEX-SaCas9-sgROSA26), GH application (3 μg/mL) caused a significant increase in the number of current-evoked action potentials in LC neurons. However, with *Ghr* knockdown, the effect of GH was largely abolished (Figure 6E). These results indicate that GH increases the intrinsic excitability of LC neurons via GHR-dependent signaling.

Activation of LC neurons is known to suppress sleep.[38–40] We thus tested the effect of GH on sleep-wake states. In mice expressing control sgRNA (sgControl), intracerebroventricular (i.c.v.) infusion of GH (40 μg/mL in artificial cerebrospinal fluid [ACSF], 2 μL) caused a significant increase in wakefulness and decrease in sleep (Figure 6F). By contrast, in mice with *Ghr* knockdown in the LC, GH infusion had no significant effect. This is consistent with c-FOS immunochemistry (Figure 6D) and the slice recording experiment (Figure 6E), suggesting that GHR expressed in LC neurons is essential for GH regulation of brain states.

DISCUSSION

In this study, we have characterized the circuit mechanism underlying bidirectional interactions between sleep and GH

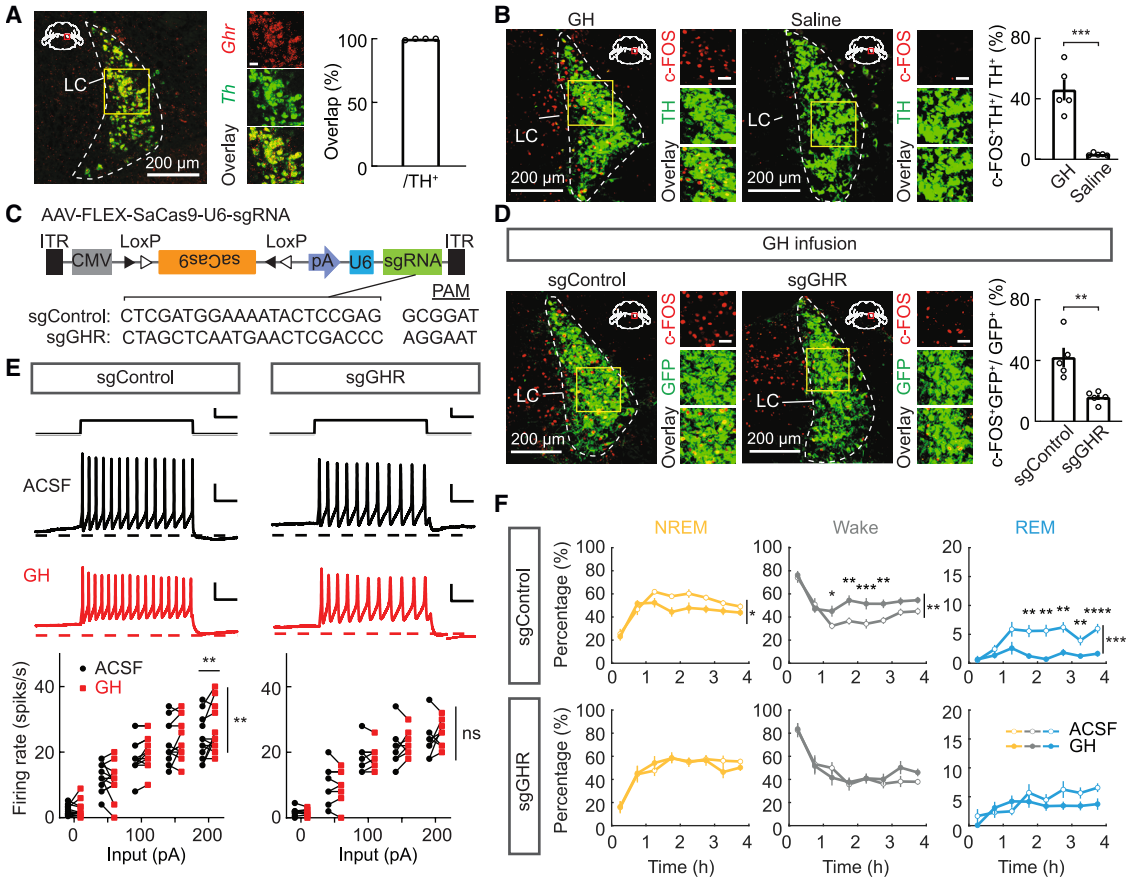


Figure 6. GH increases LC neuron excitability and regulates sleep-wake states

(A) Overlap between *Ghr* and *tyrosine hydroxylase* (*Th*) mRNA in the LC. Region in yellow box is shown on the right. Scale bar, 25 μm. The bar graph shows the percentages of TH neurons expressing *Ghr*. Each circle represents one mouse (n = 4 mice).

(B) Overlap between TH protein and c-FOS induced by saline or GH (1 μg/kg) in the LC. Regions in yellow boxes are shown on the right. Scale bar, 25 μm. The bar graph shows the percentage of TH neurons expressing c-FOS. Each circle represents one mouse (n = 5 mice per group). p = 0.0003 (t test).

(C) Viral construct used for CRISPR-Cas9-mediated gene disruption of *Ghr* (sgGHR) and *Rosa26* (sgControl).

(D) Overlap between GFP (induced by AAV-FLEX-EGFP-KASH injection in *DBH-Cre* mice) and GH-induced c-FOS in the LC in mice injected with sgControl or sgGHR virus. Regions in yellow boxes are shown on the right. Scale bar, 25 μm. The bar graph shows the percentage of GFP neurons expressing FOS after GH infusion. Each circle represents one mouse (n = 5 mice per group). p = 0.0042 (t test).

(E) Whole-cell recording from LC neurons in acute brain slices. Top, representative membrane potential traces (scale bars, 20 mV, 100 ms) in response to current steps (scale bars, 100 pA, 100 ms). Bottom, firing rate (spikes/s) during a series of current steps (0–200 pA, 500 ms) after vehicle and GH incubation. sgControl, n = 12 neurons from 10 mice. sgGHR, n = 8 neurons from 8 mice. p (sgControl) = 0.003, p (sgGHR) = 0.17 (two-way repeated measures ANOVA, treatment × input interaction). sgControl: p (200 pA) = 0.001 (Bonferroni's multiple comparisons test).

(F) Percentage of time in each brain state following vehicle or GH infusion in *DBH-Cre* mice bilaterally injected with sgControl or sgGHR virus (n = 11 mice per group). sgControl, p (NREM) = 0.018, p (wake) = 0.004, p (REM) = 0.0008. sgGHR, p (NREM) = 0.88, p (wake) = 0.74, p (REM) = 0.10 (two-way repeated measures ANOVA, main effect of treatment). sgControl-wake: p (1.5 h) = 0.021, p (2 h) = 0.004, p (2.5 h) = 0.0003, p (3 h) = 0.009; sgControl-REM: p (2 h) = 0.005, p (2.5 h) = 0.002, p (3 h) = 0.006, p (3.5 h) = 0.008, p (4 h) < 0.0001 (Bonferroni's multiple comparisons test). Error bar, ± SEM.

Bar and error bar, mean ± SEM. *p < 0.05; **p < 0.01; ***p < 0.001; ****p < 0.0001; ns, not significant.

See also Figure S6.

signaling. Combining optogenetic and chemogenetic manipulations with circuit tracing, we showed that activation of GHRH neurons in the ARC rapidly triggers GH release in a frequency-, duration-, and brain-state-dependent manner (Figure 1), whereas two populations of SST neurons suppress GH release either by inhibiting GHRH neurons or by counteracting the effect of the GHRH peptide on somatotrophs (Figures 3 and 4). Calcium fiber photometry and optrode recording revealed activity changes of both GHRH and SST neurons across sleep-wake states (Figures 2 and 5). Furthermore, we found that sleep and GH signaling interact reciprocally: while sleep enhances GH release, GH signaling promotes wakefulness by enhancing the excitability of LC noradrenergic neurons (Figure 6).

We showed that GH release is enhanced during both REM and NREM sleep (Figure 1), but through distinct mechanisms: powerful surges of both ARC GHRH and PeV SST neuron activity during REM sleep vs. a moderate shift in the balance between GHRH and SST neurons during NREM sleep (Figures 2 and 5).

Please cite this article in press as: Ding et al., Neuroendocrine circuit for sleep-dependent growth hormone release, Cell (2025), https://doi.org/10.1016/j.cell.2025.05.039

In human studies, GH release appears to be strongly associated with NREM sleep,[15,16] but in our study in mice, the overall GH levels were similar between NREM and REM sleep (Figure 1E). This divergence could be caused by differences in sleep architecture between species—sleep is fragmented in mice but consolidated in humans. Another potential factor is the difference in blood sampling frequency between studies. GH release induced by brief activation of GHRH neurons declines rapidly within a few minutes (Figure 1B); thus, a transient GH increase induced by a brief burst of GHRH activity during REM sleep could be overlooked if blood samples are collected infrequently. Furthermore, with pulsatile GH secretion,[41,42] samples collected during surges should show much higher GH levels than those taken between surges, which may contribute to the broad distribution of GH levels within each brain state (Figure 1E).

Although GHRH neuron activation strongly promotes GH release across all brain states, their optogenetic stimulation during wakefulness induced less GH release than during sleep (Figure 1D). Previous studies showed that in the presence of SST, the same amount of GHRH induces much less GH release by pituitary cells.[43,44] Since the activity of PeV SST neurons (which project to the pituitary) is higher during wakefulness (Figure 5), it is likely to reduce the efficacy of GHRH in triggering GH release, even if GHRH neurons are similarly active upon optogenetic stimulation. Besides SST, there may be additional mechanisms regulating the efficacy of GHRH neurons in inducing GH release.[45]

In addition to the well-known negative feedback loop, in which elevated GH acts on hypothalamic neuroendocrine neurons to reduce GH release,[33,35,46] we have uncovered a new feedback pathway, which involves brainstem noradrenergic neurons. GHR expression in LC noradrenergic neurons (Figure 6A) mediates GH-induced excitation of these neurons (Figures 6B–6E) and increase in wakefulness (Figure 6F), which can in turn reduce GH release. Since an important function of sleep is to promote tissue growth and regulate metabolism through GH release,[7,10,11] in addition to the circuits mediating the effect of sleep on GH release, a feedback mechanism by which GH levels influence sleep could be beneficial for optimizing this regulatory process. We found that GH signaling preferentially increases LC neuron spiking at relatively high current inputs, which are nevertheless well within the range used in previous studies of LC neurons.[47] GH application has also been shown to induce depolarization and increased spiking of agouti-related protein (AgRP) neurons in the ARC.[34] Although the cellular pathway through which GHR influences LC neuron excitability is unclear, it is likely to involve Janus kinase-signal transducer and activator of transcription (JAK-STAT) signaling.[48]

Sleep deficiency has been linked to a variety of metabolic disorders, including diabetes, obesity, and impaired muscle growth and regeneration.[49–52] GH plays a crucial role in regulating glucose and lipid metabolism as well as muscle and bone growth.[7,9,12] By measuring and manipulating the activity of hypothalamic GHRH and SST neurons across brain states, our study provides insights into the neuroendocrine mechanism governing sleep-dependent GH release. Conversely, the GH-induced excitation of sleep-suppressing noradrenergic neurons highlights a key mechanism linking the metabolic state of the animal to the propensity for sleep.

Limitations of the study

GH release is known to change with age.[42,53,54] Our study was conducted in young adult mice (2–6 months old), and in future studies it would be important to extend these experiments to both younger and older animals. In addition to SST and GHRH, which are core components of the GH axis, there are other modulators of GH release, such as glucose,[55] corticotropin-releasing hormone,[56] and ghrelin.[57] In future studies, it would be of great interest to characterize how these modulators contribute to sleep-dependent GH release. Furthermore, humans and mice exhibit marked differences in sleep architecture (consolidated vs. fragmented sleep) and circadian regulation (diurnal vs. nocturnal). The extent to which the circuit mechanisms uncovered in this study apply to humans remains to be determined.

RESOURCE AVAILABILITY

Lead contact

Further information and requests for resources and reagents should be directed to and will be fulfilled by the lead contact, Yang Dan (ydan@berkeley.edu).

Materials availability

All reagents generated in this study are available from the lead contact with a completed material transfer agreement.

Data and code availability

- All data necessary to understand and assess the conclusions of this manuscript are presented in the paper and the supplemental materials.
- Any additional information required to reanalyze the data reported in this paper is available from the lead contact upon request.

ACKNOWLEDGMENTS

We thank M. Myers for generously providing the *GHRH*-Cre mice; C. Chang for generously providing the *DBH-Cre* mice; the High-Throughput Screening Facility at the University of California Berkeley for help with ELISA; and Viral Tools, the Viral Cores at the University of North Carolina, and Addgene for supplying AAV. This work was supported by the Howard Hughes Medical Institute and the Pivotal Life Sciences Chancellor's Chair fund.

AUTHOR CONTRIBUTIONS

X.D. and Y.D. conceived and designed the study and wrote the paper with input from all authors. X.D. performed most of the experiments. F.-J.H., X. D., and P.Z. performed and analyzed slice electrophysiology experiments. D.S., B.L., and L.L. helped with calcium fiber photometry and wrote programs for data analysis. C.M., G.J., Z.Z., and X.T. helped with virus preparation and histology. X.H. and Z.M.T. helped with data analysis. J.D. provided critical consultation and assistance with slice electrophysiology. Y.D. supervised all aspects of the work.

DECLARATION OF INTERESTS

Y.D. is a member of the advisory board of *Cell*.

STAR★METHODS

Detailed methods are provided in the online version of this paper and include the following:

- KEY RESOURCES TABLE
- EXPERIMENTAL MODEL AND STUDY PARTICIPANT DETAILS
- METHOD DETAILS
  - Plasmid and virus preparation

Please cite this article in press as: Ding et al., Neuroendocrine circuit for sleep-dependent growth hormone release, Cell (2025), https://doi.org/10.1016/j.cell.2025.05.039

- Surgical procedures
- Polysomnographic recordings
- Blood sample collection and GH measurement
- Optogenetic manipulation
- Chemogenetic manipulation
- Fluorogold injection
- Fiber photometry imaging
- Fiber photometry data analysis
- Optrode recording
- Whole-cell slice electrophysiology
- GH infusion
- Histology

● QUANTIFICATION AND STATISTICAL ANALYSIS

Received: June 20, 2024
Revised: April 30, 2025
Accepted: May 28, 2025

REFERENCES

1. Van Cauter, E., Spiegel, K., Tasali, E., and Leproult, R. (2008). Metabolic consequences of sleep and sleep loss. Sleep Med. *9*, S23–S28. https://doi.org/10.1016/S1389-9457(08)70013-3.
2. Luyster, F.S., Strollo, P.J., Jr., Zee, P.C., and Walsh, J.K.; Boards of Directors of the American Academy of Sleep Medicine and the Sleep Research Society (2012). Sleep: a health imperative. Sleep *35*, 727–734. https://doi.org/10.5665/sleep.1846.
3. Mullington, J.M., Haack, M., Toth, M., Serrador, J.M., and Meier-Ewert, H.K. (2009). Cardiovascular, inflammatory, and metabolic consequences of sleep deprivation. Prog. Cardiovasc. Dis. *51*, 294–302. https://doi.org/10.1016/j.pcad.2008.10.003.
4. Mullington, J.M., Chan, J.L., Van Dongen, H.P., Szuba, M.P., Samaras, J., Price, N.J., Meier-Ewert, H.K., Dinges, D.F., and Mantzoros, C.S. (2003). Sleep loss reduces diurnal rhythm amplitude of leptin in healthy men. J. Neuroendocrinol. *15*, 851–854. https://doi.org/10.1046/j.1365-2826.2003.01069.x.
5. Spiegel, K., Tasali, E., Penev, P., and Van Cauter, E. (2004). Brief communication: Sleep curtailment in healthy young men is associated with decreased leptin levels, elevated ghrelin levels, and increased hunger and appetite. Ann. Intern. Med. *141*, 846–850. https://doi.org/10.7326/0003-4819-141-11-200412070-00008.
6. Spiegel, K., Leproult, R., and Van Cauter, E. (1999). Impact of sleep debt on metabolic and endocrine function. Lancet *354*, 1435–1439. https://doi.org/10.1016/S0140-6736(99)01376-8.
7. Møller, N., and Jørgensen, J.O.L. (2009). Effects of growth hormone on glucose, lipid, and protein metabolism in human subjects. Endocr. Rev. *30*, 152–177. https://doi.org/10.1210/er.2008-0027.
8. Kopchick, J.J., Berryman, D.E., Puri, V., Lee, K.Y., and Jorgensen, J.O.L. (2020). The effects of growth hormone on adipose tissue: old observations, new mechanisms. Nat. Rev. Endocrinol. *16*, 135–146. https://doi.org/10.1038/s41574-019-0280-9.
9. Giustina, A., Mazziotti, G., and Canalis, E. (2008). Growth hormone, insulin-like growth factors, and the skeleton. Endocr. Rev. *29*, 535–559. https://doi.org/10.1210/er.2007-0036.
10. Isaksson, O.G., Jansson, J.O., and Gause, I.A. (1982). Growth hormone stimulates longitudinal bone growth directly. Science *216*, 1237–1239. https://doi.org/10.1126/science.7079756.
11. Salomon, F., Cuneo, R.C., Hesp, R., and Sönksen, P.H. (1989). The effects of treatment with recombinant human growth hormone on body composition and metabolism in adults with growth hormone deficiency. N. Engl. J. Med. *321*, 1797–1803. https://doi.org/10.1056/NEJM198912283212605.
12. Velloso, C.P. (2008). Regulation of muscle mass by growth hormone and IGF-I. Br. J. Pharmacol. *154*, 557–568. https://doi.org/10.1038/bjp.2008.153.
13. Ayuk, J., and Sheppard, M.C. (2006). Growth hormone and its disorders. Postgrad. Med. J. *82*, 24–30. https://doi.org/10.1136/pgmj.2005.036087.
14. Kimura, F., and Tsai, C.W. (1984). Ultradian rhythm of growth hormone secretion and sleep in the adult male rat. J. Physiol. *353*, 305–315. https://doi.org/10.1113/jphysiol.1984.sp015337.
15. Sassin, J.F., Parker, D.C., Mace, J.W., Gotlin, R.W., Johnson, L.C., and Rossman, L.G. (1969). Human growth hormone release: relation to slow-wave sleep and sleep-walking cycles. Science *165*, 513–515. https://doi.org/10.1126/science.165.3892.513.
16. Takahashi, Y., Kipnis, D.M., and Daughaday, W.H. (1968). Growth hormone secretion during sleep. J. Clin. Invest. *47*, 2079–2090. https://doi.org/10.1172/JCI105893.
17. Mitsugi, N., and Kimura, F. (1985). Simultaneous determination of blood levels of corticosterone and growth hormone in the male rat: relation to sleep-wakefulness cycle. Neuroendocrinology *41*, 125–130. https://doi.org/10.1159/000124165.
18. Guillemin, R., Brazeau, P., Böhlen, P., Esch, F., Ling, N., and Wehrenberg, W.B. (1982). Growth hormone-releasing factor from a human pancreatic tumor that caused acromegaly. Science *218*, 585–587. https://doi.org/10.1126/science.6812220.
19. Rivier, J., Spiess, J., Thorner, M., and Vale, W. (1982). Characterization of a growth hormone-releasing factor from a human pancreatic islet tumour. Nature *300*, 276–278. https://doi.org/10.1038/300276a0.
20. Brazeau, P., Vale, W., Burgus, R., Ling, N., Butcher, M., Rivier, J., and Guillemin, R. (1973). Hypothalamic polypeptide that inhibits the secretion of immunoreactive pituitary growth hormone. Science *179*, 77–79. https://doi.org/10.1126/science.179.4068.77.
21. Bloch, B., Brazeau, P., Ling, N., Bohlen, P., Esch, F., Wehrenberg, W.B., Benoit, R., Bloom, F., and Guillemin, R. (1983). Immunohistochemical detection of growth hormone-releasing factor in brain. Nature *301*, 607–608. https://doi.org/10.1038/301607a0.
22. Rupp, A.C., Allison, M.B., Jones, J.C., Patterson, C.M., Faber, C.L., Bozadjieva, N., Heisler, L.K., Seeley, R.J., Olson, D.P., and Myers, M.G., Jr. (2018). Specific subpopulations of hypothalamic leptin receptor-expressing neurons mediate the effects of early developmental leptin receptor deletion on energy balance. Mol. Metab. *14*, 130–138. https://doi.org/10.1016/j.molmet.2018.06.001.
23. Steyn, F.J., Huang, L., Ngo, S.T., Leong, J.W., Tan, H.Y., Xie, T.Y., Parlow, A.F., Veldhuis, J.D., Waters, M.J., and Chen, C. (2011). Development of a method for the determination of pulsatile growth hormone secretion in mice. Endocrinology *152*, 3165–3171. https://doi.org/10.1210/en.2011-0253.
24. Ehlers, C.L., Reed, T.K., and Henriksen, S.J. (1986). Effects of corticotropin-releasing factor and growth hormone-releasing factor on sleep and activity in rats. Neuroendocrinology *42*, 467–474. https://doi.org/10.1159/000124489.
25. Kerkhofs, M., Van Cauter, E., Van Onderbergen, A., Caufriez, A., Thorner, M.O., and Copinschi, G. (1993). Sleep-promoting effects of growth hormone-releasing hormone in normal men. Am. J. Physiol. *264*, E594–E598. https://doi.org/10.1152/ajpendo.1993.264.4.E594.
26. Obal, F., Jr., Alföldi, P., Cady, A.B., Johannsen, L., Sary, G., and Krueger, J.M. (1988). Growth hormone-releasing factor enhances sleep in rats and rabbits. Am. J. Physiol. *255*, R310–R316. https://doi.org/10.1152/ajpregu.1988.255.2.R310.
27. Osterstock, G., Mitutsova, V., Barre, A., Granier, M., Fontanaud, P., Chazalon, M., Carmignac, D., Robinson, I.C.A.F., Low, M.J., Plesnila, N., et al. (2016). Somatostatin triggers rhythmic electrical firing in hypothalamic GHRH neurons. Sci. Rep. *6*, 24394. https://doi.org/10.1038/srep24394.
28. Jiang-Xie, L.F., Yin, L., Zhao, S., Prevosto, V., Han, B.X., Dzirasa, K., and Wang, F. (2019). A Common Neuroendocrine Substrate for Diverse General Anesthetics and Sleep. Neuron *102*, 1053–1065. https://doi.org/10.1016/j.neuron.2019.03.033.

Please cite this article in press as: Ding et al., Neuroendocrine circuit for sleep-dependent growth hormone release, Cell (2025), https://doi.org/10.1016/j.cell.2025.05.039

29. Kriegsfeld, L.J., Korets, R., and Silver, R. (2003). Expression of the circadian clock gene Period 1 in neuroendocrine cells: an investigation using mice with a Per1::GFP transgene. Eur. J. Neurosci. *17*, 212–220. https://doi.org/10.1046/j.1460-9568.2003.02431.x.

30. Kawano, H., and Daikoku, S. (1988). Somatostatin-containing neuron systems in the rat hypothalamus: retrograde tracing and immunohistochemical studies. J. Comp. Neurol. *271*, 293–299. https://doi.org/10.1002/cne.902710209.

31. Merchenthaler, I., Setalo, G., Csontos, C., Petrusz, P., Flerko, B., and Negro-Vilar, A. (1989). Combined retrograde tracing and immunocytochemical identification of luteinizing hormone-releasing hormone- and somatostatin-containing neurons projecting to the median eminence of the rat. Endocrinology *125*, 2812–2821. https://doi.org/10.1210/endo-125-6-2812.

32. Brooks, A.J., and Waters, M.J. (2010). The growth hormone receptor: mechanism of activation and clinical implications. Nat. Rev. Endocrinol. *6*, 515–525. https://doi.org/10.1038/nrendo.2010.123.

33. Burton, K.A., Kabigting, E.B., Clifton, D.K., and Steiner, R.A. (1992). Growth hormone receptor messenger ribonucleic acid distribution in the adult male rat brain and its colocalization in hypothalamic somatostatin neurons. Endocrinology *131*, 958–963. https://doi.org/10.1210/endo.131.2.1353444.

34. Furigo, I.C., Teixeira, P.D.S., de Souza, G.O., Couto, G.C.L., Romero, G. G., Perelló, M., Frazão, R., Elias, L.L., Metzger, M., List, E.O., et al. (2019). Growth hormone regulates neuroendocrine responses to weight loss via AgRP neurons. Nat. Commun. *10*, 662. https://doi.org/10.1038/s41467-019-08607-1.

35. Tannenbaum, G.S. (1980). Evidence for autoregulation of growth hormone secretion via the central nervous system. Endocrinology *107*, 2117–2120. https://doi.org/10.1210/endo-107-6-2117.

36. Furigo, I.C., Metzger, M., Teixeira, P.D.S., Soares, C.R.J., and Donato, J., Jr. (2017). Distribution of growth hormone-responsive cells in the mouse brain. Brain Struct. Funct. *222*, 341–363. https://doi.org/10.1007/s00429-016-1221-1.

37. Kastrup, Y., Le Grevès, M., Nyberg, F., and Blomqvist, A. (2005). Distribution of growth hormone receptor mRNA in the brain stem and spinal cord of the rat. Neuroscience *130*, 419–425. https://doi.org/10.1016/j.neuroscience.2004.10.003.

38. Antila, H., Kwak, I., Choi, A., Pisciotti, A., Covarrubias, I., Baik, J., Eisch, A., Beier, K., Thomas, S., Weber, F., et al. (2022). A noradrenergic-hypothalamic neural substrate for stress-induced sleep disturbances. Proc. Natl. Acad. Sci. USA *119*, e2123528119. https://doi.org/10.1073/pnas.2123528119.

39. Carter, M.E., Yizhar, O., Chikahisa, S., Nguyen, H., Adamantidis, A., Nishino, S., Deisseroth, K., and de Lecea, L. (2010). Tuning arousal with optogenetic modulation of locus coeruleus neurons. Nat. Neurosci. *13*, 1526–1533. https://doi.org/10.1038/nn.2682.

40. Hayat, H., Regev, N., Matosevich, N., Sales, A., Paredes-Rodriguez, E., Krom, A.J., Bergman, L., Li, Y., Lavigne, M., Kremer, E.J., et al. (2020). Locus coeruleus norepinephrine activity mediates sensory-evoked awakenings from sleep. Sci. Adv. *6*, eaaz4232. https://doi.org/10.1126/sciadv.aaz4232.

41. Labarthe, A., Zizzari, P., Fiquet, O., Lebrun, N., Veldhuis, J.D., Roelfsema, F., Chauveau, C., Bohlooly-Y, M., Epelbaum, J., and Tolle, V. (2022). Effect of Growth Hormone Secretagogue Receptor Deletion on Growth, Pulsatile Growth Hormone Secretion, and Meal Pattern in Male and Female Mice. Neuroendocrinology *112*, 215–234. https://doi.org/10.1159/000516147.

42. Ho, K.Y., Evans, W.S., Blizzard, R.M., Veldhuis, J.D., Merriam, G.R., Samojlik, E., Furlanetto, R., Rogol, A.D., Kaiser, D.L., and Thorner, M.O. (1987). Effects of sex and age on the 24-hour profile of growth hormone secretion in man: importance of endogenous estradiol concentrations. J. Clin. Endocrinol. Metab. *64*, 51–58. https://doi.org/10.1210/jcem-64-1-51.

43. Brazeau, P., Ling, N., Böhlen, P., Esch, F., Ying, S.Y., and Guillemin, R. (1982). Growth hormone releasing factor, somatocrinin, releases pituitary growth hormone in vitro. Proc. Natl. Acad. Sci. USA *79*, 7909–7913. https://doi.org/10.1073/pnas.79.24.7909.

44. Fukata, J., Diamond, D.J., and Martin, J.B. (1985). Effects of rat growth hormone (rGH)-releasing factor and somatostatin on the release and synthesis of rGH in dispersed pituitary cells. Endocrinology *117*, 457–467. https://doi.org/10.1210/endo-117-2-457.

45. Vélez, E.J., and Unniappan, S. (2020). A Comparative Update on the Neuroendocrine Regulation of Growth Hormone in Vertebrates. Front. Endocrinol. (Lausanne) *11*, 614981. https://doi.org/10.3389/fendo.2020.614981.

46. Chihara, K., Minamitani, N., Kaji, H., Arimura, A., and Fujita, T. (1981). Intraventricularly injected growth hormone stimulates somatostatin release into rat hypophysial portal blood. Endocrinology *109*, 2279–2281. https://doi.org/10.1210/endo-109-6-2279.

47. McKinney, A., Hu, M., Hoskins, A., Mohammadyar, A., Naeem, N., Jing, J., Patel, S.S., Sheth, B.R., and Jiang, X. (2023). Cellular composition and circuit organization of the locus coeruleus of adult mice. eLife *12*, e80100. https://doi.org/10.7554/eLife.80100.

48. Han, Y., Leaman, D.W., Watling, D., Rogers, N.C., Groner, B., Kerr, I.M., Wood, W.I., and Stark, G.R. (1996). Participation of JAK and STAT proteins in growth hormone-induced signaling. J. Biol. Chem. *271*, 5947–5952. https://doi.org/10.1074/jbc.271.10.5947.

49. Cappuccio, F.P., Taggart, F.M., Kandala, N.B., Currie, A., Peile, E., Stranges, S., and Miller, M.A. (2008). Meta-analysis of short sleep duration and obesity in children and adults. Sleep *31*, 619–626. https://doi.org/10.1093/sleep/31.5.619.

50. Dattilo, M., Antunes, H.K.M., Medeiros, A., Mônico-Neto, M., Souza, S., Lee, K.S., Tufik, S., and de Mello, M.T. (2012). Paradoxical sleep deprivation induces muscle atrophy. Muscle Nerve *45*, 431–433. https://doi.org/10.1002/mus.22322.

51. Gangwisch, J.E., Heymsfield, S.B., Boden-Albala, B., Buijs, R.M., Kreier, F., Pickering, T.G., Rundle, A.G., Zammit, G.K., and Malaspina, D. (2007). Sleep duration as a risk factor for diabetes incidence in a large U.S. sample. Sleep *30*, 1667–1673. https://doi.org/10.1093/sleep/30.12.1667.

52. Mônico-Neto, M., Dáttilo, M., Ribeiro, D.A., Lee, K.S., de Mello, M.T., Tufik, S., and Antunes, H.K.M. (2017). REM sleep deprivation impairs muscle regeneration in rats. Growth Factors *35*, 12–18. https://doi.org/10.1080/08977194.2017.1314277.

53. Finkelstein, J.W., Roffwarg, H.P., Boyar, R.M., Kream, J., and Hellman, L. (1972). Age-related change in the twenty-four-hour spontaneous secretion of growth hormone. J. Clin. Endocrinol. Metab. *35*, 665–670. https://doi.org/10.1210/jcem-35-5-665.

54. Edén, S. (1979). Age- and sex-related differences in episodic growth hormone secretion in the rat. Endocrinology *105*, 555–560. https://doi.org/10.1210/endo-105-2-555.

55. Stanley, S., Domingos, A.I., Kelly, L., Garfield, A., Damanpour, S., Heisler, L., and Friedman, J. (2013). Profiling of Glucose-Sensing Neurons Reveals that GHRH Neurons Are Activated by Hypoglycemia. Cell Metab. *18*, 596–607. https://doi.org/10.1016/j.cmet.2013.09.002.

56. Raza, J., Massoud, A.F., Hindmarsh, P.C., Robinson, I.C., and Brook, C.G. (1998). Direct effects of corticotrophin-releasing hormone on stimulated growth hormone secretion. Clin. Endocrinol. (Oxf.) *48*, 217–222. https://doi.org/10.1046/j.1365-2265.1998.3821204.x.

57. Kojima, M., Hosoda, H., Date, Y., Nakazato, M., Matsuo, H., and Kangawa, K. (1999). Ghrelin is a growth-hormone-releasing acylated peptide from stomach. Nature *402*, 656–660. https://doi.org/10.1038/45230.

58. Hunker, A.C., Soden, M.E., Krayushkina, D., Heymann, G., Awatramani, R., and Zweifel, L.S. (2020). Conditional Single Vector CRISPR/SaCas9 Viruses for Efficient Mutagenesis in the Adult Mouse Nervous System. Cell Rep. *30*, 4303–4316. https://doi.org/10.1016/j.celrep.2020.02.092.

Please cite this article in press as: Ding et al., Neuroendocrine circuit for sleep-dependent growth hormone release, Cell (2025), https://doi.org/10.1016/j.cell.2025.05.039

59. Hauswirth, W.W., Lewin, A.S., Zolotukhin, S., and Muzyczka, N. (2000). Production and purification of recombinant adeno-associated virus. Methods Enzymol. *316*, 743–761. https://doi.org/10.1016/s0076-6879(00)16760-6.

60. Zhang, S., Xu, M., Chang, W.C., Ma, C., Hoang Do, J.P., Jeong, D., Lei, T., Fan, J.L., and Dan, Y. (2016). Organization of long-range inputs and outputs of frontal cortex for top-down control. Nat. Neurosci. *19*, 1733–1742. https://doi.org/10.1038/nn.4417.

61. Osakada, F., and Callaway, E.M. (2013). Design and generation of recombinant rabies virus vectors. Nat. Protoc. *8*, 1583–1601. https://doi.org/10.1038/nprot.2013.094.

62. Sun, Y., Wang, P., Zheng, H., and Smith, R.G. (2004). Ghrelin stimulation of growth hormone release and appetite is mediated through the growth hormone secretagogue receptor. Proc. Natl. Acad. Sci. USA *101*, 4679–4684. https://doi.org/10.1073/pnas.0305930101.

63. Lerner, T.N., Shilyansky, C., Davidson, T.J., Evans, K.E., Beier, K.T., Zalocusky, K.A., Crow, A.K., Malenka, R.C., Luo, L., Tomer, R., et al. (2015). Intact-Brain Analyses Reveal Distinct Information Carried by SNc Dopamine Subcircuits. Cell *162*, 635–647. https://doi.org/10.1016/j.cell.2015.07.014.

64. Xu, M., Chung, S., Zhang, S., Zhong, P., Ma, C., Chang, W.C., Weissbourd, B., Sakai, N., Luo, L., Nishino, S., et al. (2015). Basal forebrain circuit for sleep-wake control. Nat. Neurosci. *18*, 1641–1647. https://doi.org/10.1038/nn.4143.

65. Blackmore, D.G., Golmohammadi, M.G., Large, B., Waters, M.J., and Rietze, R.L. (2009). Exercise increases neural stem cell number in a growth hormone-dependent manner, augmenting the regenerative response in aged mice. Stem Cells *27*, 2044–2052. https://doi.org/10.1002/stem.120.

66. Blackmore, D.G., Vukovic, J., Waters, M.J., and Bartlett, P.F. (2012). GH mediates exercise-dependent activation of SVZ neural precursor cells in aged mice. PLOS One *7*, e49912. https://doi.org/10.1371/journal.pone.0049912.

67. Zhang, Z., Zhong, P., Hu, F., Barger, Z., Ren, Y., Ding, X., Li, S., Weber, F., Chung, S., Palmiter, R.D., et al. (2019). An Excitatory Circuit in the Perioculomotor Midbrain for Non-REM Sleep Control. Cell *177*, 1293–1307. https://doi.org/10.1016/j.cell.2019.03.041.

68. Zhong, P., Zhang, Z., Barger, Z., Ma, C., Liu, D., Ding, X., and Dan, Y. (2019). Control of Non-REM Sleep by Midbrain Neurotensinergic Neurons. Neuron *104*, 795–809. https://doi.org/10.1016/j.neuron.2019.08.026.

69. Erben, L., and Buonanno, A. (2019). Detection and Quantification of Multiple RNA Sequences Using Emerging Ultrasensitive Fluorescent In Situ Hybridization Techniques. Curr. Protoc. Neurosci. *87*, e63. https://doi.org/10.1002/cpns.63.

Please cite this article in press as: Ding et al., Neuroendocrine circuit for sleep-dependent growth hormone release, Cell (2025), https://doi.org/10.1016/j.cell.2025.05.039

CellPress
OPEN ACCESS

STAR★METHODS

KEY RESOURCES TABLE

REAGENT or RESOURCE	SOURCE	IDENTIFIER
Antibodies		
Chicken anti-GFP	Aves Labs	Cat# GFP-1020; RRID: AB_10000240
Rabbit anti-c-Fos	Synaptic System	Cat# 226003; RRID: AB_2231974
Rabbit anti-TH	Abcam	Cat# ab112; RRID: AB_297840
Chicken anti-TH	Abcam	Cat# ab76442; RRID: AB_152453
Rat anti-mCherry	Thermo Fisher Scientific	Cat# M11217; RRID: AB_2536611
Bacterial and virus strains		
AAV2-EF1α-DIO-ChR2-eYFP	UNC Chapel Hill Vector Core	N/A
AAV2-EF1α-DIO-mCherry	UNC Chapel Hill Vector Core	N/A
AAV2-EF1a-DIO-GCaMP6s	UNC Chapel Hill Vector Core	N/A
AAV2-EF1a-fDIO-GCaMP6s	UNC Chapel Hill Vector Core	N/A
AAV2-EF1α-DIO-eYFP	UNC Chapel Hill Vector Core	N/A
AAV2-EF1α-DIO-hM4D(Gi)-mCherry	Addgene	44362
AAV2-EF1α-DIO-hM3D(Gq)-mCherry	Addgene	44361
AAV8-FLPX-rc [ChrimsonR-tdTomato]	Addgene	128589
AAV1-Ef1a-fDIO-tdTomato	Addgene	128434
AAV2-CAG-FLEx-TC	Gift from Liqun Luo lab, Stanford University	N/A
AAV2-CAG-FLEx-TC66T	Addgene	48331
AAV2-CAG-FLEx-RG	Addgene	74292
AAV1-hSyn1-SIO-stGtACR2-FusionRed	Addgene	105677
AAV2-CMV-FLEX-SaCas9-U6-sgGHR	This paper	N/A
AAV2-CMV-FLEX-SaCas9-U6-sgROSA26	Addgene	159914
AAV2-FLEX-EGFP-KASH	Addgene	154373
RG-deleted, eGFP-expressing rabies virus	Gene Transfer Targeting and Therapeutics Core of Salk Institute	N/A
Chemicals, peptides, and recombinant proteins		
Mouse GH / Growth Hormone Protein (Recombinant)	LSBio	LS-G131510
Clozapine-N-oxide	Sigma-aldrich	C0832
Fluorogold	Fluorochrome	Fluoro-Gold
Critical commercial assays		
RNAscope Manual Fluorescent Multiplex kit V2	Advanced Cell Diagnostics	Cat# 323100
BaseScopeTM Reagent Kit v2 – RED Assay	Advanced Cell Diagnostics	Cat# 323900
Rat/Mouse Growth Hormone ELISA kit	Millipore	Cat.EZRMGH-45K
Experimental models: Cell lines		
Hamster: B7GG cells	Gene Transfer Targeting and Therapeutics Core of Salk Institute	N/A
Hamster: BHK-EnvA cells	Gene Transfer Targeting and Therapeutics Core of Salk Institute	N/A
Human: HEK293-TVA cells	Gene Transfer Targeting and Therapeutics Core of Salk Institute	N/A
Human: HEK293T cells	Gift from Liqun Luo lab, Stanford University	N/A
Experimental models: Organisms/strains		
Mouse, *SST*^{Cre}	The Jackson Laboratory	013044; RRID: IMSR_JAX:013044

(*Continued on next page*)

Please cite this article in press as: Ding et al., Neuroendocrine circuit for sleep-dependent growth hormone release, Cell (2025), https://doi.org/10.1016/j.cell.2025.05.039

Continued

REAGENT or RESOURCE	SOURCE	IDENTIFIER
Mouse, *SST*^{Flp}	The Jackson Laboratory	031629; RRID: IMSR_JAX:031629
Mouse, *B6;129S4-Gt(ROSA)26Sor*$^{tm9(EGFP/Rpl10a)Amc/J}$	The Jackson Laboratory	024750; RRID: IMSR_JAX:024750
Mouse, *GHRH*^{Cre}	Dr. Christopher Chang (University of California Berkeley)	N/A
Mouse, *DBH*^{Cre}	Dr. Martin Myers (University of Michigan)	N/A
Oligonucleotides		
Sst In situ hybridization probe	Advanced Cell Diagnostics	40463
Ghr In situ hybridization probe	Advanced Cell Diagnostics	464951
Ghr In situ hybridization probe (Basescope)	Advanced Cell Diagnostics	1169281
Ghrh In situ hybridization probe	Advanced Cell Diagnostics	470991
Th In situ hybridization probe	Advanced Cell Diagnostics	317621
Slc32a1 In situ hybridization probe	Advanced Cell Diagnostics	319191
Single guide RNA sequence for *Ghr*: CTAGCTCAATGAACTCGACCCAGGAAT	This paper	N/A
Recombinant DNA		
pAAV-CMV-FLEX-SaCas9-U6-sgRNA	Addgene	124844
Software and algorithms		
MATLAB	MathWorks	R2020a
ImageJ	NIH	1.52a
IGOR Pro	WaveMetrics	Version 6
CellProfiler	CellProfiler	Version 4.2
KlustaKwik	Kenneth D. Harris	http://klustakwik.sourceforge.net
Synapse	TDT	Version 96

EXPERIMENTAL MODEL AND STUDY PARTICIPANT DETAILS

All procedures were approved by Animal Care and Use Committees of the University of California, Berkeley. C57BL/6J (000664), *SST-Cre* (013044), *SST-Flp* (031629), and *EGFP-L10a* (024750) mice were obtained from The Jackson Laboratory. *DBH-Cre* mice were gifts from Christopher Chang (University of California Berkeley). *GHRH-Cre* mice were gifts from Martin Myers (University of Michigan). All the experiments were performed on adult animals (2–6 months) of both genders. Mice were housed in 12 h light-dark cycles (lights on at 07:00 and off at 19:00) with free access to food and water. Animals with implants were housed individually.

METHOD DETAILS

Plasmid and virus preparation

CRISPR design tool, CRISPick (https://portals.broadinstitute.org/gppx/crispick/public) was used to select sgRNA sequences. sgRNAs with the highest score were chosen. Guide oligos were synthesized by IDT (Integrated DNA Technologies) and annealed as described.[58] sgRNA were cloned into pAAV-CMV-FLEX-SaCas9-U6-sgRNA (Addgene, plasmid #124844) accordingly. AAV2-CMV-FLEX-SaCas9-U6-sgGHR, AAV2-CMV-FLEX-SaCas9-U6-sgROSA26 (Addgene, plasmid #159914) and AAV2-FLEX-EGFP-KASH (Addgene, plasmid # 154373) were prepared by Janelia Viral Tools. AAV2-EF1α-DIO-hM4D(Gi)-mCherry (Addgene, #44362), AAV2-hSyn-DIO-hM3D(Gq)-mCherry (Addgene, #44361), AAV1-Ef1a-fDIO-tdTomato (Addgene, #128434), AAV1-hSyn1-SIO-stGtACR2-FusionRed (Addgene; #105677), and AAV8-FLPX-rc [ChrimsonR-tdTomato] (Addgene; #128589) were obtained from Addgene. AAV2-EF1a-DIO-hChR2-eYFP, AAV2-EF1a-DIO-GCaMP6s, and AAV2-EF1a-fDIO-GCaMP6s were obtained from the University of North Carolina (UNC) vector core. AAV2-CAG-FLEx-TC66T (Addgene, plasmid #48331) and AAV2-CAG-FLEx-RG (RG, rabies glycoprotein; Addgene, plasmid #74292) were prepared in-house according to previously described protocols.[59,60] RG-deleted, eGFP-expressing rabies virus (RVdG) was purchased from Gene Transfer Targeting and Therapeutics Core of Salk Institute, amplified in B7GG cells, pseudotyped with BHK-EnvA cells, and titered with HEK293-TVA cells.[61] The final titer of all the viruses was estimated to be $\geq 1 \times 10^{12}$ gc/ml.

Please cite this article in press as: Ding et al., Neuroendocrine circuit for sleep-dependent growth hormone release, Cell (2025), https://doi.org/10.1016/j.cell.2025.05.039

Surgical procedures

For all the surgeries, mice were anesthetized with 1.5%–2% isoflurane and placed on a stereotaxic frame. A heat pad was used to keep the body temperature stable during the procedure. Eye ointment was applied to prevent drying. After shaving the furs and sterilizing the scalp with Betadine and medical alcohol, an incision was made to the skin to expose the skull.

For EEG and EMG recordings, EEG recordings were made from two stainless steel screws on top of the right and left cortex, at anteroposterior (AP) –3.5 mm, mediolateral (ML) 3 mm, and AP -2 mm, ML 3 mm, respectively. Two EMG electrodes were inserted into the neck musculature. A reference screw was inserted into the skull above the cerebellum. Insulated leads from the EEG and EMG electrodes were soldered to a pin header, which was secured to the skull using dental cement.

For optogenetic activation experiments, a craniotomy (0.5-1mm diameter) was made on top of the target regions (see below for coordinates), and 100-150 nl virus was injected into the target region using Nanoject II (Drummond Scientific) via a micropipette. Optic fibers (Neurophotometrics, 200 μm core, 0.37 NA) were implanted into the target region two weeks after viral injection. Dental cement was applied to cover the exposed skull completely and to secure the implants for EEG and EMG recordings to the screws. For optogenetic inhibition experiments, 150 nl virus was injected into the target region bilaterally. For chemogenetic experiments, 100-150 nl AAV2-hSyn-DIO-hM3D(Gq)-mCherry was injected into the target region.

For saCas9-mediated gene disruption, 300 nl of mixed AAV2-FLEX-EGFP-KASH and AAV2-CMV-FLEX-SaCas9-U6-sgROSA26 or AAV2-CMV-FLEX-SaCas9-U6-sgGHR was injected into the target region bilaterally. Mice were not tested until 2 months after the injection.

For GH infusion experiments, a customized guide cannula (P1Technologies) was inserted into the lateral ventricle. The cannula was secured to the skull with EEG and EMG electrodes using dental cement.

For rabies-mediated retrograde transsynaptic tracing, 150 nl of mixed AAV2-CAG-FLEx-TC66T (local) or AAV2-CAG-FLEx-TCB (long-distance) and AAV2-CAG-FLEx-RG was injected into the ARC. Three weeks later, RVdG pseudotyped with EnvA was injected into the same region, and mice were sacrificed 6 days later for histology.

For dual calcium fiber photometry recording two craniotomies (0.5–1 mm in diameter) were made (see below for coordinates), 250 nl of AAV2-EF1a-fDIO-GCaMP6s was injected into the PeV and 100-150 nl of AAV2-EF1a-DIO-GCaMP6s was injected into the ARC of *GHRH-Cre; SST-Flp* mice. Optical fibers (Neurophotometrics, 200 μm core, 0.37 NA) with FC ferrule were implanted into PeV on the left hemisphere and ARC on the right hemisphere 2 weeks later and secured to the skull with EEG and EMG electrodes using dental cement.

For optogenetics combined with calcium fiber photometry, 150 nl of mixed AAV2-EF1a-DIO-GCaMP6s and AAV8-FLPX-rc [ChrimsonR-tdTomato] or AAV1-Ef1a-fDIO-tdTomato was injected into the ARC of *GHRH-Cre; SST-Flp* mice. Optical fibers (Neurophotometrics, 200 μm core, 0.37 NA) with FC ferrule were implanted into the same region 2 weeks later and secured to the skull with EEG and EMG electrodes using dental cement.

For optrode recording experiments, a custom-made optrode assembly was inserted into the ARC region. The optrode assembly was secured to the skull together with EEG and EMG electrodes using dental cement.

After surgery, mice were allowed to recover from anesthesia on a heating pad before being returned to their home cage. Buprenorphine (0.1 mg/kg) was given prior to surgery, and meloxicam (5–10 mg/kg) was given prior to surgery and once the following day. All experiments were carried out at least one week after surgery.

Stereotaxic coordinates for virus injection and optic fiber or guide cannula implantation:

Lateral ventricle: AP +0.1 mm, ML 0.9 mm, DV 2.5 mm
PeV: AP -0.4 mm, ML 0.3 mm, DV virus injection: 4.7 and 4.9 mm; fiber implantation: 4.6 mm
ARC: AP -1.8 mm, ML 0.3 mm, DV virus injection: 5.9 mm; fiber implantation: 2-degree angle, 5.7 mm
LC: AP -5.5 mm, ML 0.9 mm, DV 3.8 mm

Polysomnographic recordings

Behavioral experiments were carried out in home cages placed in sound-attenuating boxes. EEG and EMG electrodes were connected to flexible recording cables via a mini-connector. Recordings started after 20-30 min of habituation. The signals were recorded with a TDT RZ5 amplifier (bandpass filter, 1-750 Hz; sampling rate, 1,500 Hz). Spectral analysis was carried out using fast Fourier transform (FFT), and brain states were classified into NREM, REM, and wake states (wake: desynchronized EEG and high EMG activity, NREM: synchronized EEG with high-amplitude, low-frequency (0.5-4 Hz) activity and low EMG activity, REM: high power at theta frequencies (6-9 Hz) and low EMG activity). The classification was performed using a custom-written graphical user interface (programmed in MATLAB, MathWorks).

Blood sample collection and GH measurement

Tail-clip blood sample collection was performed as previously described.[23] Briefly, to minimize stress, mice were habituated to the handling and tail manipulation for 7 days, 15 min each day by the same person conducting all subsequent experiments. Before the first sample collection, a small portion of the tail tip (1 mm) was cut with a surgical blade to allow the collection of small drops of blood. All blood collections were done in home cage. For each blood collection, a 2.5 μl sample of whole blood was collected and mixed with

Please cite this article in press as: Ding et al., Neuroendocrine circuit for sleep-dependent growth hormone release, Cell (2025), https://doi.org/10.1016/j.cell.2025.05.039

7.5 μl of PBS with 5 mM EDTA. Samples were immediately placed on dry ice and stored at −80 °C for later analysis. Gentle pressure was applied with gauze to the wound to stop the blood flow at the end of a collection. For subsequent blood withdrawals, the surface of the original wound was disrupted (mechanically or by applying gauze soaked in physiological saline). These experiments were conducted during the light phase, and comparisons were made between sleep and wake states within the same circadian window, thereby ruling out circadian influences.

For optogenetic activation experiments with different laser frequencies, blood samples were collected at 2, 4, 6, 8, 10, 15, 20, and 30 min after laser onset. For optogenetic activation experiments with different laser durations, blood samples were collected at 1, 2, 3, and 4 min after laser onset. Blood samples for time 0 were collected immediately before laser onset. Animals remained awake during the experiment.

For optogenetic activation and inhibition during different brain states, experiments were done during the light phase. EEG and EMG were recorded. Blood samples were collected 2 min after laser onset. The sleep recordings were later analyzed and blood samples were assigned to different brain states. To measure endogenous GH release (not evoked by laser), blood samples were collected every 1-2 hours during the light phase. The sleep recordings were later analyzed. Blood samples were assigned to different brain states. Samples collected during or immediately after feeding were excluded to avoid potential GH release triggered by hunger or food intake.[62] REM samples refer to those collected during REM sleep or within 60 s after a REM episode.

Total blood collected from each animal per day is < 25 μl. The whole blood GH level was determined by Rat/Mouse Growth Hormone ELISA kit from Millipore according to the manufacturer's instructions (Cat.EZRMGH-45K).

Optogenetic manipulation

Each optic fiber was attached through an FC/PC adaptor to a 473-nm blue laser diode (Shanghai laser), and light pulses were generated using the TDT system. For GHRH optogenetic activation experiments, each trial consisted of a 5 Hz pulse train (10 ms per pulse) lasting for 120 s. The laser power was 6 mW/mm^2 at fiber tip. In each optogenetic manipulation experiment, inter-trial interval was chosen randomly from a uniform distribution between 10 and 14 min, regardless of which brain state the animal is in. Each experimental session lasted for 3-4 hours, and each animal was tested in 5-6 sessions.

For optogenetic activation of GHRH neurons, the laser power was 6 mW/mm^2 at fiber tip. To test the frequency-dependent GH release, 2, 5, 10, or 20 Hz pulse train (10 ms per pulse) were applied for 120 s. To test the duration-dependent GH release, 10 Hz pulse train (10 ms per pulse) was applied for 2, 10, 20, 40, 60, or 120 s. For optogenetic stimulation of GHRH neurons during different brain states, 5 Hz pulse train (10 ms per pulse) was applied for 40 s. The inter-trial interval is greater than 2 hours. For optogenetic activation of SST neurons, 20 Hz pulse train (10 ms per pulse) was applied for 2 min. For optogenetic inhibition of GHRH neurons, constant laser (10 mW/mm^2) was applied for 2 min.

For optogenetic activation applied with fiber photometry, a 635 nm collimated diode laser system (Laserglow, D631001FL) was attached through an FC/PC adaptor. Each trial consisted of a 20 Hz pulse train (30 ms per pulse) lasting for 60 s. The laser power was 10 mW/mm^2 at fiber tip.

Chemogenetic manipulation

Saline (0.9% NaCl) or Clozapine N–oxide (CNO, Sigma, C0832; 1 mg/kg) was intraperitoneally injected into mice expressing hM3D (Gq)-mCherry / hM4D(Gi)-mCherry / mCherry in the ARC or PeV at 7:00 pm (onset of the dark phase). Data were averaged across mice for statistical comparisons. Each recording session started immediately after injection. In each test set, mice received saline and CNO in a random sequence. Each mouse was subjected to 3-4 test sets, and the data were averaged across all sets. For tail-clip blood sample collection, blood samples for time 0 were collected before the CNO or saline injection. For the SST neuron inhibition experiments (Figures 4F and 4G), the mice were mostly awake due to CNO injection and blood collection. For the sleep deprivation group, mice were kept awake by lightly tapping on the cages. To reduce the possibility of stress, mice were never touched directly.

Fluorogold injection

As previously described,[28,29] mice received a subcutaneously injection of 50 μl 5% Fluorogold (Fluorochrome,Denver, Colorado) in saline and were sacrificed 6 days later for histology.

Fiber photometry imaging

Fiber photometry was performed using a TDT RZ10x real-time processor. Mice were in their home cages placed in sound-attenuating boxes, and were attached via an optical fiber (Neurophotometrics, 200 μm core, 0.37 NA) implanted in the ARC/PeV to a 6-port fluorescence Mini Cube (Doric Lenses; FMC6) during fiber photometry imaging. Fluorescence elicited by 405 nm (serving as an isosbestic wavelength for GCaMP6s) and 465 nm (calcium-dependent GCaMP6s fluorescence) LEDs was filtered through the Doric minicube and collected with an integrated photosensor on the RZ10x. Signals were pre-processed using the TDT Synapse software and collected at a sampling frequency of 1018 Hz. For optogenetic activation combined with fiber photometry, a 635 nm collimated diode laser system (Laserglow, D631001FL) was connected to the Doric Mini Cube. Light pulses (10 mW/mm^2 at fiber tip, 20 Hz, 60 s) were generated using the TDT Synapse software and the inter-trial interval was set randomly from a uniform distribution between 600 and 900 s.

Please cite this article in press as: Ding et al., Neuroendocrine circuit for sleep-dependent growth hormone release, Cell (2025), https://doi.org/10.1016/j.cell.2025.05.039

Fiber photometry data analysis

The 405-nm channel was used to correct nonspecific, calcium-independent changes in fluorescence, e.g., movement artifacts. Each channel (465-nm and 405-nm) was first fit with a single exponential to remove the baseline change due to bleaching. The 405-nm signal was then fit to the 465-nm signal using a least-squares linear fit method and then subtracted from the 465-nm signal.[63] The resulting signals were then converted to z-scores based on the mean and standard deviation of the entire recording session. Each recording session lasted for 3-4 hours. The response amplitude was computed as the average of laser stimulation period after subtracting the baseline period (0 to 100 s before laser onset).

Optrode recording

Custom-made optrodes consisted of an optic fiber (200 μm in diameter) glued together with 6 pairs of stereotrodes. Two FeNiCr wires (Stablohm 675, California Fine Wire), which were twisted together and electroplated to an impedance of ~200 kΩ using a custom-built plating device. The optrode was attached to a driver to allow vertical movement of the optrode assembly. Wires to record cortical EEG and EMG from neck musculature were also attached for simultaneous recordings. A TDT RZ5 amplifier was used for all the recordings, signals were filtered (0.3–8 kHz) and digitized at 25 kHz. At the end of the experiment, an electrolytic lesion was made by passing a current (100 μA, 10 s) through one or two electrodes to identify the end of the recording tract.

Spikes were sorted offline based on the waveform energy and the first three principal components of the spike waveform on each stereotrode channel. Single units were identified automatically using the software KlustaKwik (http://klustakwik.sourceforge.net). The quality of each unit was assessed by the presence of a refractory period and quantified using isolation distance and L-ratio. Units with an isolation distance < 20 and L-ratio > 0.1 were discarded.

To identify ChR2-tagged neurons, laser pulse trains (15 and 30 Hz with duration of 1 and 0.5 s, respectively) were delivered every 1 or 2 min. A unit was identified as ChR2 expressing if spikes were evoked by laser pulses with high reliability (> 0.7 for all units in our sample), short first-spike latency (< 8 ms for all units in our sample), low jitter (< 3 ms for all units in our sample), and the waveforms of the laser-evoked and spontaneous spikes were highly similar (correlation coefficient > 0.9). To calculate the average firing rate of each unit in each brain state, spikes during the laser pulse trains were excluded.

Whole-cell slice electrophysiology

300 nl of mixed AAV2-FLEX-EGFP-KASH and AAV2-CMV-FLEX-SaCas9-U6-sgROSA26 or AAV2-CMV-FLEX-SaCas9-U6-sgGHR was injected into the LC of *DBH-Cre* or *DBH-Cre;EGFP-L10a* mice bilaterally. Recordings were made at least 2 months after injection. Slice was prepared according to procedures described previously.[64] Briefly, mouse was deeply anesthetized with 5% isoflurane. After decapitation, the brain was dissected rapidly in ice-cold artificial cerebrospinal fluid (ACSF) containing (in mM) 125 NaCl, 2.5 KCl, 1.25 NaH2PO4, 25 NaHCO3, 15 glucose, 2 CaCl2, and 1 MgCl2, with continuous bubbling with 95% O2 and 5% CO2 (300-305 mOsm, pH 7.4). Coronal slices (250 μm thickness) containing locus coeruleus were made with a vibratome (Leica). Slices were then incubated for 30 min in 34 °C ASCF for recovery and then held at room temperature. For recordings, slices were transferred to a recording chamber, held in place with an anchor (Warner Instrument), and mounted onto a microscope (BX51, Olympus) equipped and a 40x water-immersion objective (Olympus). The slices were continuously perfused with ACSF at a rate of 2-3 ml/min at 30 °C during recording, and brain slices were recorded within 4 hours after recovery.

For whole-cell current-clamp, glass pipettes (2.5-4.5 MΩ) were filled with internal solution containing (in mM) 135 KMeSO3, 5 KCl, 10 HEPES, 4 Mg-ATP, 0.3 Na3-GTP, 8 Na2-phosphocreatine, 1 EGTA, 0.1 CaCl2 (280-290 mOsm, adjusted to pH 7.3-7.4). Cells with series resistance >25 MΩ were excluded. Step currents (500 ms) from 0 pA to 200 pA were used to evoke AP firing before and after GH incubation (3 μg/ml, 15 min). Recordings were made through a Multiclamp 700B amplifier (Molecular Devices) and monitored with Clampex (Molecular Devices) software. The signal was low-pass filtered at 2.2 kHz and digitized at 10 kHz (Digidata 1440a, Molecular Devices).

GH infusion

For FISH or immunohistochemistry samples, GH (1 μg/kg, LS-G131510, LSBio) or saline was delivered via retro-orbital injection to mice under brief anesthesia. Animals were sacrificed 2 hours after the infusion for histological analysis. For sleep behavior recording, mice with a guide cannula inserted into the lateral ventricle were intracranially microinjected with GH (40 ng/μl in ACSF, 2 μl, similar to the amount used in previous studies[65,66]) or ACSF into the ventricle at a rate of 0.2 μl/min. After a 10-minute waiting period, the infusion cannula was detached. In each test set, mice were administered ACSF and GH in a randomized sequence. Each mouse underwent 3-4 test sets, and the data were averaged across all sets.

Histology

Mice were deeply anesthetized and transcardially perfused with 0.1 M PBS, followed by 4% paraformaldehyde (w/v) in PBS. Brains were post-fixed overnight in 4% paraformaldehyde. For cryoprotection, brains were immersed in a 30% sucrose (w/v) PBS solution for 36-48 hours. After embedding and freezing, brains were sectioned into 30-μm slices (for FISH and a subset of immunohistochemistry) or 50-μm slices (for other immunohistochemistry) using a cryostat.

For immunohistochemistry, brain slices were washed three times with PBS, permeabilized with PBST (0.3% Triton X-100 in PBS) for 30 minutes, and then incubated with a blocking solution (5% normal goat serum in PBST) for 1 hour. Subsequently, brain slices

were incubated overnight at 4°C with primary antibodies: anti-GFP (GFP-1020, Aves Labs, 1:500), anti-TH (ab112, ab76442, Abcam, 1:500), and anti-cFos (226008, SYNAPTIC SYSTEMS, 1:500). Some brain slices underwent antigen retrieval pre-treatment. On the following day, the slices were washed with PBS and incubated with appropriate secondary antibodies for 2 hours (1:1000, All from Invitrogen): A-11039, Alexa Fluor 488 goat anti-chicken IgG; A-11012, Alexa Fluor 594 goat anti-rabbit IgG; A-21244, Alexa Fluor 647 goat anti-rabbit IgG. FISH was performed using RNAscope Multiplex Fluorescent Assays V2 or BaseScope Reagent Kit v2 – RED Assay according to the manufacturer's instructions (Advanced Cell Diagnostics), in some cases, followed by immunostaining to detect TH and GFP. Fluorescence images were captured using a fluorescence microscope (Keyence BZ-X710).

QUANTIFICATION AND STATISTICAL ANALYSIS

Data analysis was performed in MATLAB, IGOR Pro 6.0 (WaveMetrics), CellProfiler, and ImageJ. Statistical analysis was performed using MATLAB and GraphPad. The brain state was scored with 5-s bins. Probability of each brain state in each time bin (before, during, after laser stimulation or following saline or CNO injection) was computed as the percentage of recording time spent in each state in that time bin; the probabilities for wake, NREM, and REM add up to 100% for all time bins. All statistical tests were two-sided. Data are shown as means ± SEM unless otherwise stated. The 95% confidence intervals (CI) for brain state probabilities were calculated using a bootstrap procedure as previously described.[67,68] RNAscope and BaseScope results were analyzed using CellProfiler as recommended by Advanced Cell Diagnostics and previously described.[69] For other comparisons, tests were provided in the text or figure legends.

CellPress
OPEN ACCESS

Supplemental figures

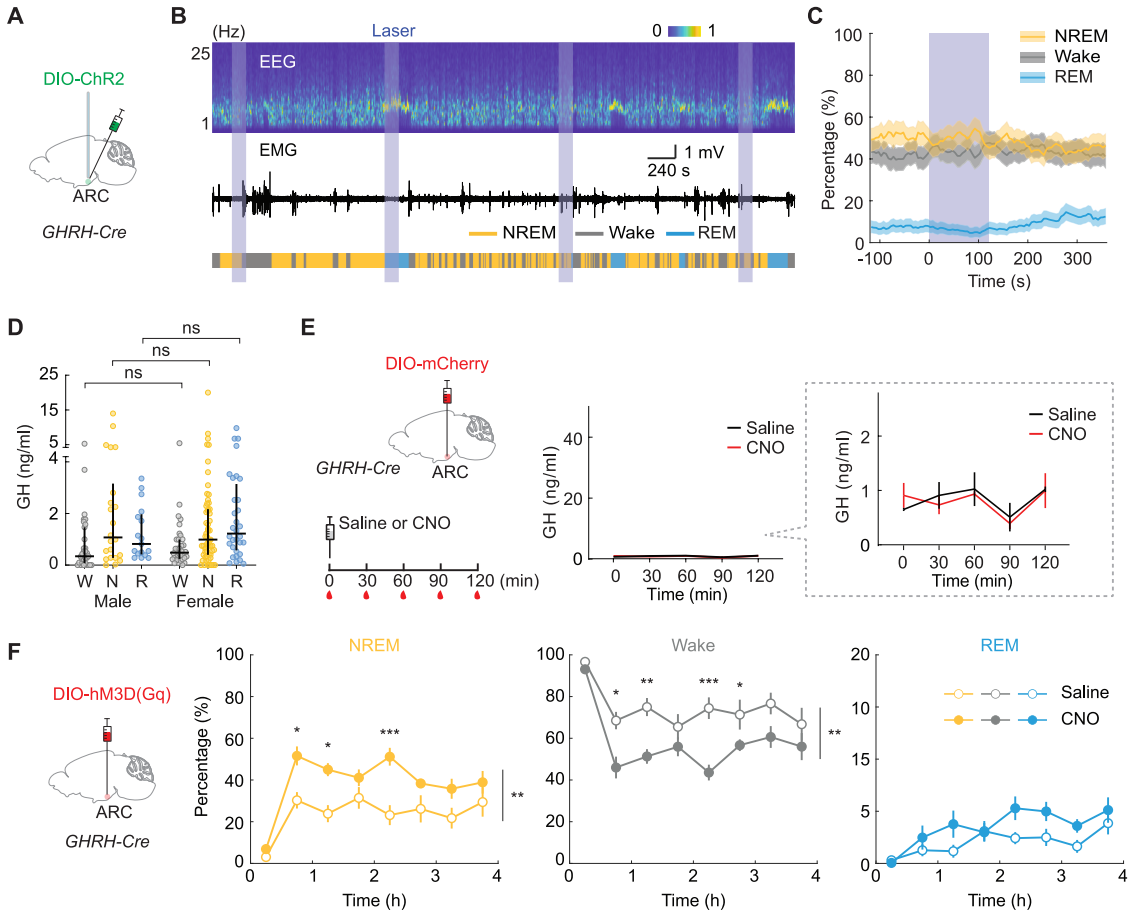


Figure S1. Effects of optogenetic activation (5 Hz) and chemogenetic activation of GHRH neurons on brain states and GH level after saline/CNO injection in control *GHRH-Cre* mice expressing mCherry only, related to Figure 1

(A) Schematic of optogenetic stimulation in *GHRH-Cre* mice expressing ChR2-eYFP in the ARC.

(B) An example optogenetic activation experiment with EEG spectrogram, EMG trace, and brain states (color-coded). Blue stripe, laser stimulation period (5 Hz, 120 s).

(C) Percentage of time in NREM, REM, or wake state before, during, and after laser activation of GHRH neurons (n = 5 mice). Shading, 95% confidence intervals (CIs). Blue stripe, laser stimulation period (5 Hz, 120 s).

(D) GH levels in blood for male and female mice. Male: wake, n = 31 samples; NREM, n = 22; REM, n =17; from 5 mice. p (wake vs. NREM) = 0.034, p (wake vs. REM) = 0.11, p (NREM vs. REM) > 0.99. Female: wake, n = 36 samples; NREM, n = 59; REM, n = 32; from 8 mice. p (wake vs. NREM) = 0.035, p (wake vs. REM) = 0.004, p (NREM vs. REM) = 0.83. Male vs. female: p (wake vs. wake) > 0.99, p (NREM vs. NREM) > 0.99, p (REM vs. REM) > 0.99 (Kruskal-Wallis test followed by Dunn's test). Horizontal bar, median; vertical bar, first (top) and third (bottom) quartiles. ns, not significant.

(E) Left, schematic of ARC expressing mCherry in GHRH neurons. Middle, GH levels were measured before and after saline or CNO injection, with or without sleep deprivation (n = 6 mice). Right, GH levels with scaled y axis.

(F) Left, schematic of chemogenetic activation of *GHRH-Cre* mice expressing hM3D(Gq)-mCherry in the ARC. Right, percentage of time in each brain state following CNO or saline injection (n = 7 mice). Horizontal axis: time after CNO/saline injection. p (NREM) = 0.008, p (wake) = 0.008, p (REM) = 0.13 (two-way repeated measures ANOVA, main effect of treatment). NREM: p (1 h) = 0.04, p (1.5 h) = 0.01, p (2.5 h) = 0.0004; wake: p (1 h) = 0.046, p (1.5 h) = 0.007, p (2.5 h) = 0.0004, p (3 h) = 0.04 (Bonferroni's multiple comparisons test).

Error bar, ± SEM; shading, ± SEM. *p < 0.05; **p < 0.01; ***p < 0.001; ns, not significant.

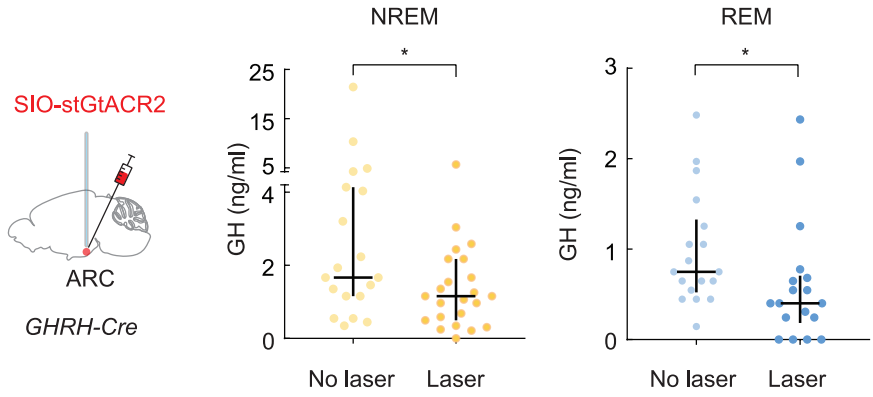


Figure S2. GH levels in blood measured after 2 min of optogenetic inhibition of GHRH neurons, related to Figure 2

Left, schematic of optogenetic inhibition in *GHRH-Cre* mice expressing stGtACR2-FusionRed in the ARC. Middle, inhibition during NREM sleep. *n* (no laser) = 19 samples; *n* (laser) = 23 samples from 4 mice; $p = 0.043$. Right, inhibition during REM sleep. *n* (no laser) = 18 samples; *n* (laser) = 18 samples from 4 mice. $p = 0.016$ (Mann-Whitney test).

Horizontal bar, median; vertical bar, first (top) and third (bottom) quartiles. *$p < 0.05$.

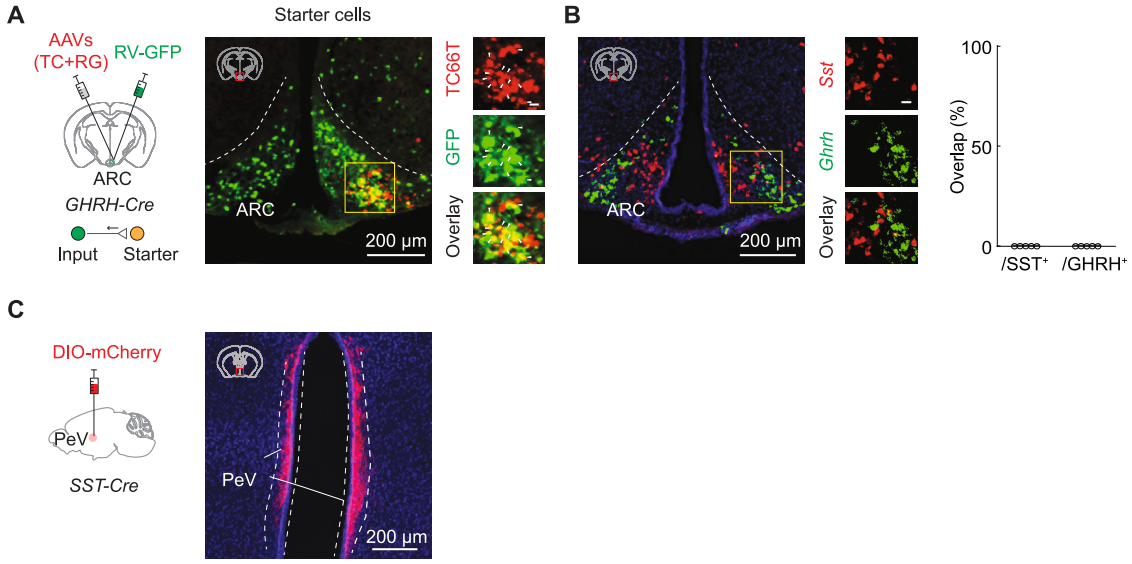


Figure S3. Starter cells in the ARC in RV tracing experiment; overlap between GHRH and SST neurons, related to Figure 3

(A) Left, schematic showing rabies-mediated transsynaptic tracing from ARC GHRH neurons. Right, fluorescence image of starter cells in the ARC (expressing both GFP and TC66T). Region in yellow box is shown on the right. Scale bar, 25 μm. Arrowheads indicate co-labeled neurons.

(B) Overlap between *Ghrh* and *Sst* mRNA in the ARC. Region in yellow box is shown on the right. Scale bar, 25 μm. The bar graph shows the percentages of SST and GHRH neurons that are co-labeled. Each circle represents one mouse (n = 5 mice).

(C) Left, schematic of *SST-Cre* mice injected with AAV-DIO-mCherry in the PeV. Right, an example fluorescence image of mCherry expressed in the PeV of an *SST-Cre* mouse.

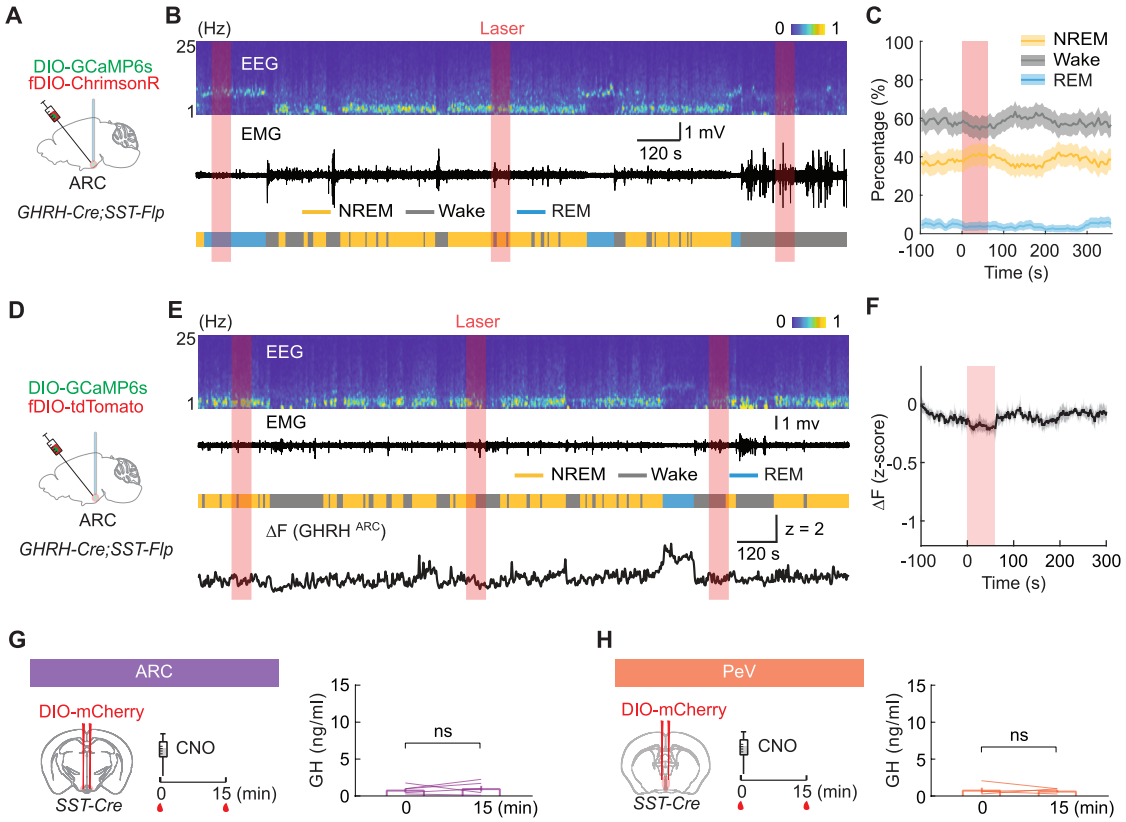


Figure S4. Effect of activating ARC SST neurons on brain states; laser stimulation of SST neurons in control mice without ChrimsonR; GH level after saline/CNO injection in control *SST-Cre* mice expressing mCherry only, related to Figure 4

(A) Schematic of calcium fiber photometry and optogenetic manipulation through the same fiber.

(B) An example session with EEG spectrogram, EMG trace, and brain states (color-coded). Red stripe, laser stimulation period (20 Hz, 60 s).

(C) Percentage of time in the NREM, REM, or wake state before, during, and after laser activation of ARC SST neurons, averaged from 5 mice. Shading, 95% confidence intervals (CIs). Blue stripe, laser stimulation period (20 Hz, 60 s).

(D) Schematic of calcium fiber photometry and optogenetic manipulation through the same fiber in control mice without ChrimsonR.

(E) An example session with EEG spectrogram, EMG trace, brain states (color-coded), and calcium activity of GHRH neuron. Red stripe, laser stimulation period (20 Hz, 60 s).

(F) Mean calcium activity of GHRH neurons before, during, and after laser stimulation in control mice ($n = 6$ mice). Red stripe, laser stimulation period (20 Hz, 60 s).

(G) Left, schematic of ARC expressing mCherry in SST neurons. GH levels were measured before and 15 min after CNO injection ($n = 5$ mice). $p = 0.67$ (paired t test).

(H) Similar to (G), but for mice expressing mCherry in PeV SST neurons ($n = 4$ mice). $p = 0.75$ (paired t test).

Bar and error bar, mean ± SEM. Shading, ± SEM. ns, not significant.

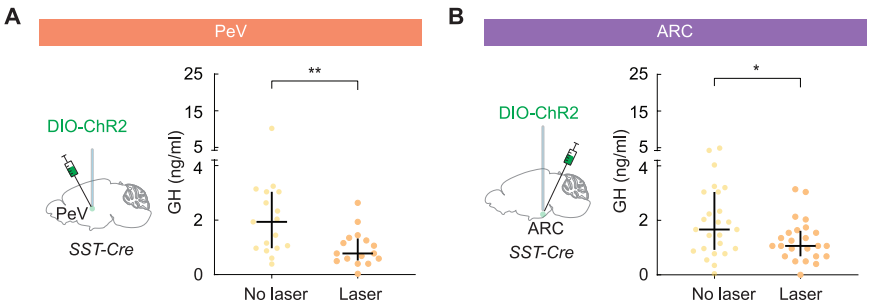


Figure S5. Blood GH levels were measured after 2 min of optogenetic activation of SST neurons, related to Figure 5

(A) Left, schematic of PeV expressing ChR2 in SST neurons. GH levels were measured after 2-min optogenetic activation of PeV SST neurons during NREM sleep. *n* (no laser) = 17 samples; *n* (laser) = 16 samples from 4 mice; $p = 0.0089$ (Mann-Whitney test).

(B) Similar to (A), but for mice expressing ChR2 in ARC SST neurons. *n* (no laser) = 25 samples, *n* (laser) = 24 samples from 5 mice; $p = 0.028$ (t test).

Horizontal bar, median; vertical bar, first (top) and third (bottom) quartiles. $^{*}p < 0.05$, $^{**}p < 0.01$.

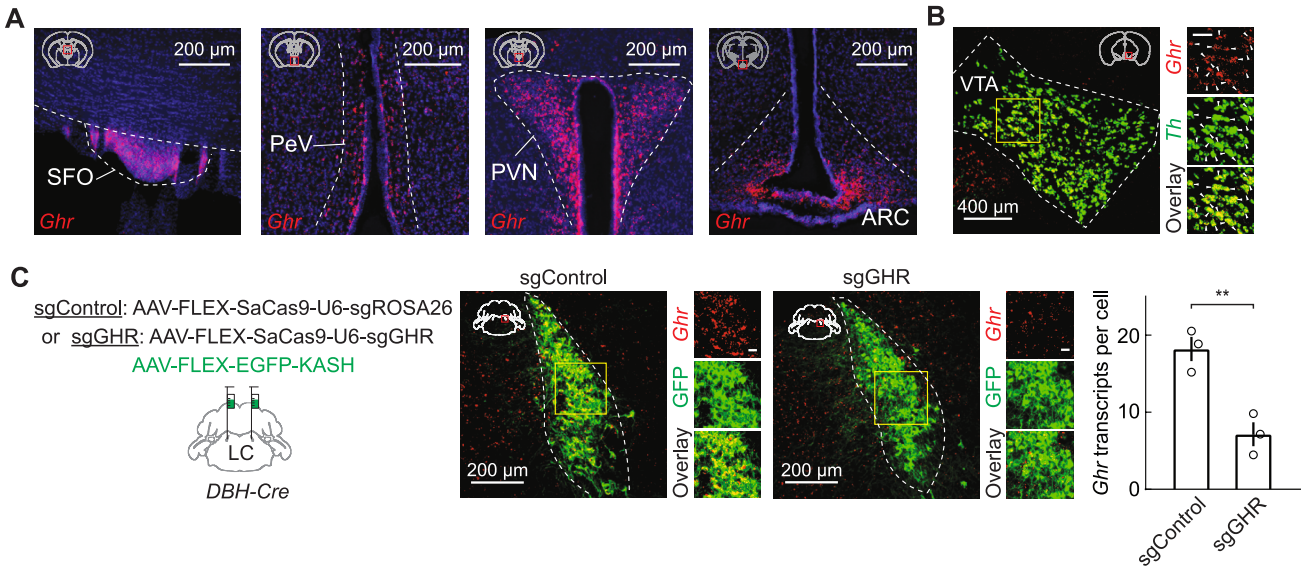


Figure S6. GHR expressions in several brain regions; BaseScope validation of *Ghr* gene disruption efficiency, related to Figure 6

(A) *Ghr* mRNA in the subfornical organ (SFO), PeV, paraventricular nucleus of the hypothalamus (PVN), and ARC.

(B) Overlap between *Ghr* and *Th* mRNA in the ventral tegmental area (VTA). Region in yellow box is shown on the right. Arrowheads indicate co-labeled neurons. Scale bar, 25 μm.

(C) Left, schematic of bilateral virus injection into the ARC of *DBH-Cre* mice. Middle, GFP protein based on immunohistochemistry and *Ghr* mRNA based on BaseScope in the LC. Regions in yellow boxes are shown on the right. Scale bar, 25 μm. Right, the bar graph shows the number of *Ghr* transcripts per cell. Each circle represents one mouse (n = 3 mice). p = 0.0074 (t test). Bar and error bar, mean ± SEM. $^{**}p < 0.01$.